THE UNIVERSITY OF MICHIGAN

INDUSTRY PROGRAM OF THE COLLEGE OF ENGINEERING

REDUCTION OF ALUMINUM OXIDE TO ALUMINUM IN RADIO FREQUENCY GENERATED PLASMAS

Roger K. Rains

A dissertation submitted in partial fulfillment
of the requirements for the degree of
Doctor of Philosophy in
The University of Michigan

April, 1968

IP - 816

ACKNOWLEDGMENTS

The author wishes to express his gratitude to all those persons who have aided in this investigation.

The interest, guidance and criticism offered by Professor Robert H. Kadlec, chairman of the doctoral committee, were especially appreciated. The interest and assistance of the other members of the doctoral committee: Professors E. E. Hucke (co-chairman), S. W. Churchill, A. A. Gordus, O. F. Kimball and R. D. Pehlke are also acknowledged.

The author is appreciative of the cooperation and help given by the secretaries and shop personnel of the Department of Chemical and Metallurgical Engineering. He is also grateful for the assistance given by his friends in the plasma laboratory.

The author is indebted to his wife and parents for their encouragement and help and to the Bethlehem Steel Corporation for its financial support of this project.

TABLE OF CONTENTS

TABLE OF CONTENTS (Continued)

TABLE OF CONTENTS (Continued)

LIST OF TABLES

LIST OF FIGURES

LIST OF FIGURES (Continued)

ABSTRACT

The reduction of aluminum oxide to aluminum in radio frequency generated, induction-coupled plasmas was experimentally investigated. The objective was to demonstrate that appreciable conversions of stable metallic oxides, such as alumina, could be obtained in an induction plasma reactor.

The reduction was effected by feeding alumina into Ar, Ar-H_2, Ar-CO and Ar-CH_4 plasmas. The plasmas were contained in a water-cooled quartz reactor and flowed downward. The products were collected on the reactor wall and on water-cooled quench probes placed directly in the plasma. The conversion of Al_2O_3 to Al was based on the amount of aluminum and aluminum oxide actually collected since complete recovery of the products was not attempted. In argon plasmas, the conversion was investigated as a function of Al_2O_3 particle size, Al_2O_3 mass flow rate and power input to the plasma. The effect of quenching the reaction mixture in a reducing atmosphere was determined by introducing H_2, CO and CH_4 into the lower section of the plasma countercurrent to the plasma flow.

The products were positively identified by x-ray diffraction and wet chemical techniques. In addition, the gaseous plasma reaction zones were examined spectroscopically to give some insight as to the nature of the gas-solid reaction. Finally, mean aluminum and argon temperatures in the plasma were determined.

In an atmospheric argon plasma flowing at 52 gm/min, the alumina conversion was enhanced by increasing the percent of vaporization of

the oxide. This was achieved by increasing the power input, and decreasing the alumina flow rate and particle size. Conversions of 3-30 percent were obtained with power levels of 5.03, 5.86 and 6.69 kw; oxide flow rates of 0.03 to 0.6 gm/min; and particle diameters of 26μ, 37μ and 45μ. The argon temperatures measured at these power levels are 10,900°, 11,100° and 11,200°K respectively. The conversions qualitatively agree with the extents of vaporization predicted by computer solutions of heat, mass and momentum balances for alumina particles. Spectroscopic identification of Al and AlO in the cooler plasma regions and only Al in the hot plasma core confirmed that vaporization of Al_2O_3 to Al in an argon plasma is a two step process: the oxide dissociates to AlO and O and the AlO in turn dissociates to Al and O .

With CO and CH_4 in the plasma, the respective conversions were 46 and 42 percent. The corresponding conversions for pure argon plasmas at similar operating conditions were 23 and 9 percent. The use of CO and CH_4 as quench gases doubled the conversions that were obtained without them. Hydrogen, in each application, had little effect. Higher conversions were obtained with the product collected on the quench probes than with that collected on the reactor wall.

Examination of the reduction product from Ar and Ar-CO plasmas identified Al, α-Al_2O_3 and γ-Al_2O_3 . The product from an Ar-CH_4 plasma also contained Al_4C_3 . No solid aluminum suboxides or aluminum oxycarbides were found.

The mean aluminum temperatures obtained for various experimental conditions ranged from 2000 to 6000°K. These results were

somewhat low and inconsistent, but it was possible to ascertain that the Al temperature increased with increasing power input and decreasing Al_2O_3 flow rate.

The reduction of stable metallic oxides, such as Al_2O_3, in induction-coupled plasmas is certainly feasible. By using CO or CH_4; increasing the power input; and decreasing the oxide flow rate and particle size, conversions of 50 percent or more should be realizable, depending upon the efficiency of the recovery of the product.

1. INTRODUCTION

The area of plasma chemistry can best be described by Searcy's Laws:[67]

1. At high temperatures, everything reacts with everything.
2. The higher the temperature, the more rapidly everything reacts.
3. The products may be anything.

It was with this concept in mind that this thesis was undertaken.

When it was decided to investigate the plasma reduction of a metallic oxide, aluminum oxide was chosen for four reasons. First, Al_2O_3 is extremely difficult to reduce and is on a par with CeO_2, Ce_2O_3, La_2O_3, Nd_2O_3, Pr_2O_3, Sc_2O_3, Sm_2O_3 and Y_2O_3 in this respect,[41] to name but a few. So if Al_2O_3 can be reduced, then a host of other oxides can also be reduced, yielding much more lucrative products. Second, since "the products may be anything," reduction of alumina itself may provide one or more products of considerable interest. Third, Al_2O_3 is inexpensive and much more readily available than most of the other difficult-to-reduce oxides. Fourth, it was felt that the two known attempts at reducing alumina had not been pursued sufficiently with the proper variables in mind.

The conversion of Al_2O_3 to Al in this study was effected in radio frequency generated, induction-coupled Ar, Ar-H_2, Ar-CO and Ar-CH_4 plasmas. Different quench techniques and three reaction variables were investigated. The specific experimental program is outlined in Chapter 4.

2. SURVEY OF PREVIOUS WORK

2.1 Reduction of Metallic Oxides in a Plasma

The literature on plasma reduction of metallic oxides is quite sparse, although it is known that several groups of researchers have investigated the area. The reason is that the majority of this work has been done by private industry.

Grosse, et al.,[47,85] attempted to reduce 200 mesh (74μ) commercial C.P. grade alumina in an arc plasma jet. Using argon plasmas, they tried Al_2O_3 flow rates of 1.5-6.0 gm/min, power inputs of 8.55-9.6 kw and total gas flow rates of 20.4-27.5 liters/min. The oxide was fed into the plasma flame (below the arc) with H_2 or CH_4 as the carrier gas. Aluminum metal was definitely formed, but the yields were very poor, ranging from 0.2 to 1.25 percent.

As an extension of the above work, Stokes, et al.,[86] studied the reductions of WO_3, Fe_2O_3, Ta_2O_5, Al_2O_3, TiO_2 and ZrO_2 in an arc plasma jet. Using He plasmas of 34 liters/min, they obtained maximum metal yields of 95 percent for WO_3 , 100 percent for Fe_2O_3 and 25.6 percent for Ta_2O_5 . The respective powder flow rates were 1.96, 0.3 and 1.9 gm/min at corresponding power levels of 15.2, 15.5 and 15.75 kw. The oxides were introduced into the plasma flame with H_2 flowing at 13.6 liters/min. Commercial grade oxide powder of unreported size was used in each of these investigations and the products of the first two reductions were of submicron size and highly pyrophoric. Conversions of 2-5 percent were achieved with 325 mesh (44μ) Al_2O_3 in He plasmas operating at power levels of 11.4-14.9 kw. The powder flow was varied

over the range 0.48 to 2.5 gm/min. At the lowest flow rate, the oxide was mixed with carbon and carried into the plasma flame in an argon stream. With oxide flows of 0.5 gm/min or greater, hydrogen was the carrier gas. No reductions were obtained with 325 mesh TiO_2 at powder flow rates of 0.4-0.6 gm/min or with ZrO_2 of unreported size flowing at 0.8 gm/min.

Brown[12] was able to reduce ZrO_2 to Zr in Ar-C and Ar-H_2 arc plasmas. He found little advantage in the use of hydrogen and found no effect due to the method of carbon introduction. There was no reduction when either 60 mesh (250μ) or 100 mesh (150μ) particles of zirconia were used, but with 10μ zirconia, the zirconium content was increased from 66.5 percent for the injected material to 70 percent for the product. This amounts to a conversion of about 21 percent.

2.2 Other Plasma Reductions of Interest

Stokes, et al.,[86] also investigated the carbothermic reduction of WO_3 to W_2C, WC and W and the reduction of Ta_2O_5 to TaC. In each case the oxide was carried in a methane stream of 6.5 liters/min into the "flame" of a helium plasma jet flowing at 34 liters/min. The WO_3 flow rates were in the range 0.51 to 4 gm/min while the operating power was varied from 10.0 to 16.3 kw. The percent conversions obtained were 9.2 - 34.6 for W_2C, 4.1 - 11.0 for WC and 43.2 - 80.8 for W. A conversion to TaC of 9.7 percent was achieved for Ta_2O_5 flowing at 0.5 gm/min at an operating power of 15.75 kw.

The decomposition of volatile metal halides has been studied by Biggerstaff, et al.,[6] and by Brown.[12] The former found that the

decompositions of boron trichloride and trifluoride in a plasma jet could be used to produce boron of very small particle size. The addition of hydrogen to the plasma did not significantly increase the conversion to the metal. Brown reduced zirconium tetrachloride in an argon plasma and tried both a hydrogen dilution quench and a straight thermal quench. With a reactant containing 38.2 percent Zr, he obtained a product with a 58.4 percent Zr content. As with Biggerstaff and his associates, he found little benefit in the use of hydrogen.

The final plasma reduction of interest was performed by Huska and Clump,[58] who studied the decomposition of MoS_2 in an induction-coupled argon plasma. Operating with MoS_2 flow rates of 0.666, 1.19 and 2.48 gm/hr and several plasma power levels between 1.9 and 5.15 kw, they obtained conversions ranging from 25.7 to 70.2 percent. The conversion increased with decreasing reactant feed rate and increased with increasing plasma energy content.

2.3 Suboxide Species of Aluminum

The gaseous oxides of aluminum have been quite extensively investigated. According to Brewer and Searcy,[11] there are only two important gaseous oxides of aluminum. Al_2O is the primary gaseous suboxide when alumina is heated under reducing conditions and AlO is the principal gaseous product under neutral or oxidizing conditions. The bulk of the remaining work, which is discussed below, substantiates their findings.

De Maria, et al.,[24] report that the main reaction upon heating Al_2O_3 from 2300 to 2600°K is the decomposition to AlO and O.

Zhadanova and Sokolov[91] and Allen, et al.,[2] found only AlO and Al when aluminum burned in oxygen and air. Thus, only AlO was observed under the neutral and oxidizing conditions of the investigations.

Porter, et al.,[75] Cochran[17] and Gastinger[36] each report formation of Al_2O when Al_2O_3 and Al were heated together. Grossman[48] heated Nb with Al_2O_3 and Grube, et al.,[49] heated Si with Al_2O_3 to form Al_2O. Worrell,[90] Motzfeldt[71] and Ponomarev, et al.,[74] obtained Al_2O by carbothermic reduction of alumina and Mal'tsev[66] formed Al_2O by carbothermic reduction of sodium and potassium hydroaluminates. Each of these are examples of reducing conditions and Al_2O is the product.

Some disagreement is offered by Inghram, et al.,[59] who found that Al_2O and Al were the major species obtained by heating Al_2O_3 under neutral conditions in a tungsten cell. Further contention is given by Hasapis, et al.,[51] who vaporized Al_2O_3 by itself in a tungsten cell and with tungsten powder. For each case, they found AlO and Al_2O in about equal concentrations. Ackermann and Thorn[1] also heated alumina in a tungsten cell and found a reaction between the two at high temperatures. However, they did not establish the nature of their products, which they thought were Al_2O and WO_3.

The literature on the existence of solid suboxides of aluminum is quite controversial. By means of a high temperature x-ray technique, Hoch and Johnson[55] found solid Al_2O between 1100 and 1500°C, solid AlO above 1600° and both from 1500 to 1600°C. They determined that both are cubic and that upon cooling or rapid quenching both compounds dissociate to Al and Al_2O_3. Cochran[17] contends that the lowered

melting points of Al_2O_3 mixed with Al indicates subcompound formation in the condensed phase. His data were too scattered to allow a phase diagram to be constructed. Khodak and Mal'tsev[61] heated $Na_2O \cdot Al_2O_3 \cdot 2SiO_2 \cdot nH_2O$ with carbon. Rapid chilling of the reaction mixture enabled them to confirm the formation of the solids Al_2O and SiO by isolation of Al_2O crystals. Beletskii and Rapoport[4] report the formation of coarse hexagonal crystals, believed to be Al_2O, when they heated Al and Al_2O_3 in the presence of SiO_2 and carbon. However, Brewer[10] believes that the substance may be a ternary Al-O-C compound.

Brewer, in this same paper, reports that he, Searcy and McCullough were unable to find a new solid phase upon room temperature x-ray examination of fused mixtures of Al and Al_2O_3. Gitleson, et al.,[40] could detect no indication of a solid suboxide either by microscopic examination or by x-ray powder patterns of solidified Al-Al_2O_3 melts. In studies of the carbothermic reduction of alumina, Emlin, et al.,[32] Foster, et al.,[34] Ginsberg and Sparwald[39] and Gitleson, et al.,[40] could find no low melting substances except the oxycarbides Al_2OC and Al_4O_4C.

2.4 Heating of Solids in a Plasma

Chludzinski[15] determined heat transfer coefficients for axisymmetric stagnation point heat transfer at thermocouple tips in argon and argon-nitrogen plasmas. With a thermocouple 0.02 inches in diameter in an argon plasma at about 10,900°K, he obtained a maximum heat transfer coefficient of 87 BTU/hr-ft^2-°F. In a 90 percent Ar-10

percent N_2 plasma at about 11,400°K, the maximum heat transfer coefficient was 162 BTU/hr-ft^2-°F. He compared the convective and radiative contributions to the heat transfer from the plasma and found the former to predominate.

Heat flux measurements were made on small argon plasma jets by Stokes, et al.,[87] who obtained heat fluxes as high as 4.5 kcal/cm^2-sec for the transient heating of a small copper slug. This corresponds to a heat transfer coefficient of about 4000 BTU/hr-ft^2-°F. Reed[77] made heat transfer intensity measurements in argon and argon with oxygen or helium induction plasmas. For the various plasmas, he obtained peak intensities of 56 to 145 watts/cm^2 for heat transfer from the tail of the plasma to the surface of a water-cooled plate. The corresponding range of approximate heat transfer coefficients is 18 to 46 BTU/hr-ft^2-°F.

Engelke[33] developed an idealized model for heat transfer to solid particles in an arc plasma stream. He compared his "integrated heat transfer to the particle" with observations on the melting of some carbides and found substantial agreement with his theory. In an argon-hydrogen plasma at 10,300°K, he noted that 250 mesh (62μ) TiC did not begin to melt whereas the smaller 625 mesh (20μ) TiC had vaporized somewhat. In a lower energy argon plasma, even the 625 mesh TiC did not begin to melt. Titanium carbide melts at 3410°K and boils at 4570°K.[56]

Loo and Dimick,[65] Meyer[70] and Wood and Wise[89] investigated the catalytic activity of some metals and oxides on the recombination of atoms with atoms and ions with electrons. Loo and Dimick conducted experiments with an argon arc flame and ascertained that metals

tend to increase the Ar^{+}-e^{-} recombination rate while oxides tend to decrease the rate. Meyer found that metallic oxides are slightly active and metals are extremely active in catalyzing recombination processes in argon-nitrogen plasmas. Wood and Wise determined that metals catalyze the recombination of H, N and O atoms.

High-speed cinematographic studies of metallic and metallic oxide powders (including Al_2O_3) in an induction-coupled argon plasma were carried out by Hedger and Hall.(52) They observed that vaporization occurred preferentially from the lower side of the descending particles and that the vaporization impeded heat transfer to the particles. It was also noted that the majority of the particles pass straight through the turbulent plasma, but a small portion is ejected from the plasma center.

3. DISCUSSION OF PREVIOUS WORK

3.1 Plasma Reduction Reactions

The success obtained with WO_3, Fe_2O_3, and Ta_2O_5 demonstrates that the use of plasmas for reducing metallic oxides is feasible. However, these oxides normally are not difficult to reduce. The use of plasmas would be much more justifiable if it would result in significant conversions for the less reducible oxides, such as Al_2O_3, TiO_2 and ZrO_2. These three oxides, for which Stokes and his associates obtained negligible reduction, have generally been considered to be much too stable to allow significant success. In other words, the oxides would reform during the quenching of the reaction mixture. So unless an extremely rapid quench could be attained, most of the metal would be lost due to this recombination.

The above argument is certainly meritorious, but one of equal importance is the ease of vaporization of the oxide. If the oxide is not vaporized and decomposed to its elements, then there is no need to worry about recombination during the quench. It is significant that WO_3, Fe_2O_3 and Ta_2O_5 are all more easily vaporized than Al_2O_3, TiO_2 or ZrO_2.[41]

Brown's work, which occurred at about the same time as the experimental portion of this thesis, demonstrates the effect of increasing the extent of vaporization of the oxide. He found no reduction of the larger 250 and 100μ ZrO_2 particles, but got a 21 percent conversion with 10μ zirconia, which was more vaporized. Thus it is reasonable to expect that Al_2O_3 and TiO_2 can also be significantly reduced if small enough particles are used.

Two other variables, viz. powder flow rate and power input to the plasma, were shown to have an effect upon the reduction of metallic compounds by the work of Huska and Clump. It is also certain that the use of a reducing gas in the plasma should improve the conversion.

3.2 Aluminum Suboxides

The majority of the studies of gaseous aluminum suboxides agree that Al_2O predominates in a reducing atmosphere and AlO in a neutral or oxidizing environment. It is further agreed that these are the only two important gaseous aluminum oxides.

A closer examination of the dissenting reports will show them to be in accord with the above conclusions. Brewer and Searcy heated alumina in a tungsten cell for their neutral conditions and found only AlO. Inghram, Hasapis, et al., and Ackermann and Thorn performed similar experiments and found Al_2O. But Ackermann and Thorn also observed a reaction between the tungsten cell and the alumina. This gave them reducing instead of neutral conditions and explains their Al_2O formation. It appears that Inghram and Hasapis, et al., also had this tungsten-alumina reaction while Brewer and Searcy, due to somewhat different conditions, had no interaction.

The controversy over the existence of solid aluminum suboxides can also be resolved to some extent. The two claims that stable solid suboxides were prepared at room temperature involved the reduction of Al_2O_3 by carbon. In the other four investigations of carbothermic reduction of alumina, the oxycarbides Al_2OC and Al_4O_4C were the products. Furthermore, when systems containing Al and Al_2O_3 without carbon were

examined at room temperature, no low melting compounds were observed. This suggests that the reported solid aluminum suboxides were actually oxycarbides.

The formation of solid suboxides at higher temperatures is very probable. Hoch and Johnson agree with Cochran that subcompounds exist in Al-Al_2O_3 systems above 1100°C and no one has disputed their claims. Nevertheless, some more high temperature studies should be made before these results can be completely accepted.

3.3 Heating of Solids in a Plasma

The heat transfer studies of Chludzinski, Stokes, et al., and Reed produced heat transfer coefficients ranging from 18 to 4000 BTU/hr-ft^2-°F. Such a wide range is reasonable since three different systems were used. The coefficients estimated from Reed's results (18-46 BTU/hr-ft^2-°F) should be at the low end because he investigated the tail of an induction flame, which is the coolest part. Chludzinski's results (87-162 BTU/hr-ft^2-°F) should be higher than Reed's because he used thermocouples which were placed in the hot core of the plasma. The small copper slugs studied by Stokes and his co-workers were also in contact with the hotter part of the plasma. The coefficient corresponding to their maximum heat flux (4000 BTU/hr-ft^2-°F) is reasonable for very small slugs since the coefficient should increase with a decrease in diameter as Chludzinski found for his thermocouples.

Engelke's observations of the melting and vaporization of TiC particles also indicate an increase in heat transfer with a decrease in particle diameter. However, his claim that 625 mesh TiC did not

begin to melt in his argon plasma is dubious. If Chludzinski's results for argon plasmas are applied to Engelke's model, at least partial melting is predicted. Such partial melting would be difficult to detect by examination of particles that had passed through the plasma.

It is concluded from the catalysis studies that metallic oxides decrease the Ar^{+}-e^{-} recombination rate and slightly increase the rate of atom-atom recombinations. Metals have the effect of increasing the rates of both types of recombination. This means that the heat transfer to oxides and metals, and hence their rate of vaporization, is affected in the same way. Two other phenomena which influence the vaporization of solids in a plasma are: its preferential occurrence at the lower side of the particle and the formation of a vapor shield around the particle. Both diminish the rate of vaporization.

4. SCOPE OF THE PRESENT STUDY

The primary aim of this research was to investigate the reduction of Al_2O_3 to Al in a radio frequency generated, induction-coupled argon plasma. It was also intended to demonstrate that an induction-coupled plasma reactor is especially suitable for such gas-solid reactions. To accomplish these goals, the following program was completed:

1. Qualitative analysis of the reaction zones with an optical spectroscope.
2. Positive identification of the products.
3. Investigate various quench methods.
4. Determine mean Al and Ar temperatures in the center of the plasma.
5. Study the effects of particle size, Al_2O_3 mass flow rate and power input to the plasma.
6. Use H_2, CO and CH_4 as reducing agents in argon plasmas.
7. Solve heat, mass and momentum balances for an Al_2O_3 particle.

The above program was designed to provide fundamental information about plasma reduction of alumina and to define the operating parameters. The purpose of the qualitative spectroscopic analysis was to acquire a better understanding of the vaporization of Al_2O_3 and quenching of the gaseous mixture. According to the literature, Al_2O_3 should decompose to AlO and this spectroscopic analysis would

be a check. The positive identification of the reduction products was necessary because the previous work on solid suboxides of aluminum suggested that it might be possible to form these compounds by a rapid quench of the gaseous suboxides.

The quench methods used were: straight thermal quench on the water-cooled reactor wall; thermal quench on a water-cooled probe placed inside the plasma; counter-current introduction of H_2, CO and CH_4 into the bottom of the plasma through the quench probe. A basic interpretation of the quench process was obtained through an understanding of why the conversion of Al_2O_3 varied as it did with changes in the Al temperature and concentration in the plasma.

The argon temperatures were used to evaluate the thermal conductivity, viscosity, density and heat capacity for the argon plasma and for the boundary layer surrounding a solid particle. These properties were used in a correlation for the heat transfer coefficient which was needed in order to solve the heat, mass and momentum balance equations. Solution of these equations allowed the time-temperature history of the particle and its extent of vaporization with axial position to be estimated.

Solids flow rate and power input to the plasma were shown to be significant variables in Section 3.1. It was also thought that particle size would be an important variable (this was later substantiated, as discussed in Section 3.1) and so the effect of these three variables on the conversion of Al_2O_3 was investigated. The reducing gases (H_2, CO and CH_4) were used in independent studies aimed at increasing the conversions above those attainable in the argon plasma.

5. THEORETICAL CONSIDERATIONS

5.1 Thermodynamics

It was established in Sections 2.3 and 3.2 that AlO and Al_2O are the only two gaseous oxides of aluminum. Furthermore, when Al_2O_3 is heated, it decomposes to AlO and O under neutral or oxidizing conditions and to Al_2O and O in a reducing atmosphere. So Al_2O_3 should vaporize to AlO and O in an argon plasma and to Al_2O and O in an argon plasma containing H_2, CO, or CH_4.

According to Brewer and Searcy,[11] the dissociation:

$$Al_2O_3 \rightarrow 2AlO + O \qquad (5.1)$$

occurs at 3800 ± 200°K. This is in fair agreement with the findings of Coheur[20] and Coheur and Coheur,[18,19] who observed that the optimum temperature for formation of AlO was 4000°C. They found that the molecule is unstable above this temperature and below it the probability of formation is slight. However, Figure 1, which was prepared from information presented in the JANAF tables,[27] shows that AlO should be stable down to about 1100°K once it is formed and is unstable above 4400°K. Since temperatures in excess of this are to be expected in an argon plasma, the AlO formed from the vaporization of Al_2O_3 should further dissociate:

$$AlO \rightarrow Al + O \qquad (5.2)$$

shortly after its formation.

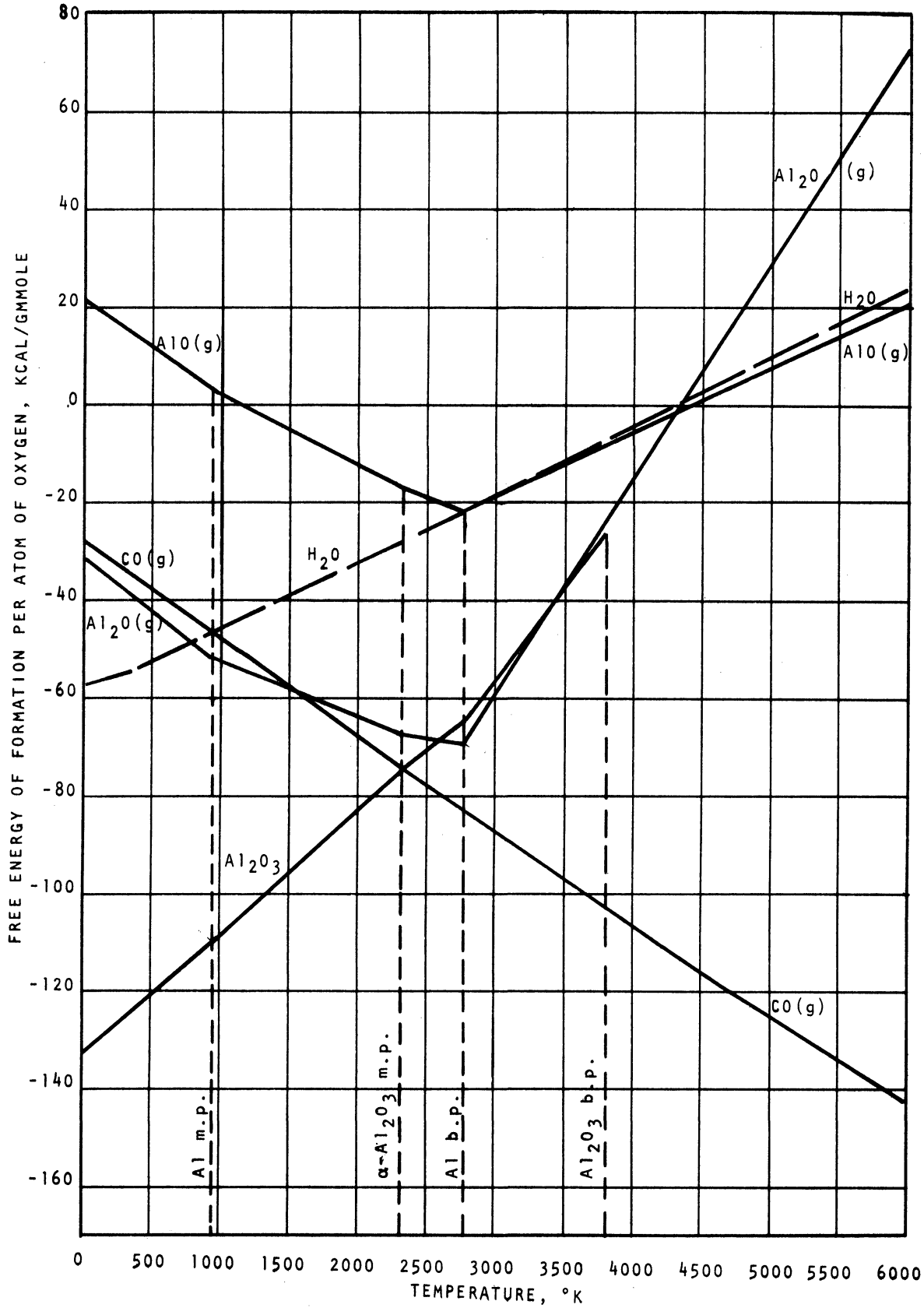

Figure 1. Free Energy of Formation per Atom of Oxygen Versus Temperature for Various Compounds.

Once Al_2O is formed it is stable below 4300°K and unstable above it, as Figure 1 shows. So if Al_2O is formed in $Ar-H_2$, Ar-CO and $Ar-CH_4$ plasmas by:

$$Al_2O_3 \rightarrow Al_2O + O \ , \tag{5.3}$$

it should also undergo a decomposition:

$$Al_2O \rightarrow 2Al + O \ . \tag{5.4}$$

In either case, therefore, the plasma should contain Al and O atoms instead of AlO or Al_2O molecules.

The use of reducing gases in the plasma is expected to aid in the quench process. This is done by removing oxygen during the quench; thus diminishing the chance that the gaseous Al will oxidize to AlO or Al_2O . Figure 1 shows that carbon is much better in this respect than hydrogen as CO is considerably more stable than H_2O over a wide temperature range. Oxygen also prefers carbon to aluminum, as seen by a comparison of the free energies of formation of CO, AlO and Al_2O . Hydrogen, on the other hand, has less affinity for oxygen than does aluminum over fairly large ranges in temperature. Consequently, hydrogen should be of little benefit in maintaining Al during the quench and carbon should be effective. Although Al_2O_3 is more stable than even CO at low temperatures, quenching occurs rapidly enough that the formation of alumina should be slight.

5.2 An Interpretation of the Quench Process

The ultrahigh temperatures of a vortex stabilized, induction-coupled argon plasma extend in the radial direction very nearly to the

wall of the cylindrical confining chamber.[15] The boundary layer between the reactor wall and the point at which the plasma temperature noticeably begins to decrease is the quench region. The concentration and temperature gradients in this quench boundary layer are extremely steep and the condensation of a species out of the plasma is a rate process controlled by these gradients.

Let us consider the case of condensation of gaseous Al from an argon plasma containing the gaseous species: Al, O, Ar and various ions of these atoms. During the quench, the following reactions should occur:

$$Al + O \rightleftarrows AlO \tag{5.5}$$

$$O + O \rightleftarrows O_2 \tag{5.6}$$

$$Al + \frac{1}{2} O_2 \rightleftarrows AlO \tag{5.7}$$

$$Al_{(g)} \rightarrow Al_{(l)} \tag{5.8}$$

as well as the recombinations of ions with electrons. Since recovery of aluminum is the purpose of the quench, it is desirable to increase the rate of transport of Al through the boundary layer so that less of it can be oxidized.

The radial molar flux of Al in a mixture of Al and the noncondensable gases is:

$$N_{Alr} = - \frac{C\, D_{Alm}}{1-X_{Al}} \frac{\partial X_{Al}}{\partial r} \tag{5.9}$$

where N_{Alr} = radial molar flux of Al ,

X_{Al} = mole fraction of Al ,

D_{Alm} = effective binary diffusivity for Al in the mixture,[8]

C = total concentration.

Since only Al condenses, the bulk flow due to the other gases was neglected in the derivation of Equation (5.9), which is found in Appendix I.

It is seen from Equation (5.9) that the molar flux of Al depends on both the concentration and temperature of aluminum (D_{Alm} is temperature dependent). If the bulk concentration of Al is increased, N_{Alr} is initially greater. But since the quench occurs with extreme rapidity, the result is that more Al is recovered. A similar argument holds for the temperature effect. The diffusion of Al atoms through a mixture depends on the temperature of the atoms; D_{Alm} increases with temperature. Therefore N_{Alr} also increases with Al temperature and again, more aluminum should be recovered. It is concluded that one means of improving the recovery of Al from an Al-O-Ar plasma is by increasing the concentration and/or the temperature of the aluminum in the plasma.

5.3 Heat, Mass and Momentum Balances

The history of a small Al_2O_3 particle in an argon plasma is estimated from a solution of steady state heat, mass and momentum balance equations for the particle. The description is only approximate because some simplifying assumptions are used in deriving the equations (see Appendix II). The use of more exact equations is not justified since a rough comparison with the experimental results is sufficient for this work.

The momentum balance derived for a small particle injected into the plasma is:

$$\frac{d^2z}{dt^2} = \pm \frac{3}{4} C_D \frac{\rho_\infty}{d_s \rho_s} \left(\frac{dz}{dt} - v_\infty \right)^2 + g \qquad (5.10)$$

where $\frac{dz}{dt}$ = velocity of solid particle,

ρ_s = density of solid particle,

d_s = diameter of solid particle,

ρ_∞ = density of bulk plasma,

v_∞ = velocity of bulk plasma,

g = gravitational acceleration,

C_D = drag coefficient.

The direction of the drag force on the particle depends on the velocity of the particle relative to the plasma ($dz/dt - v_\infty = v_{rel}$). If the relative velocity, v_{rel}, is positive, the minus sign is used in Equation (5.10) and if v_{rel} is negative, the plus sign is used.

It is assumed that the particle is spherical and remains so after melting commences. The plasma density is obtained from the ideal gas law (which is very nearly true at plasma temperatures) and a mean particle density is used. A constant average plasma velocity and Christiansen's[16] drag coefficient data are also used. Magnetic drag and slip flow effects are negligible.[80]

The heat balance for a particle as it is being heated to its vaporization temperature is:

$$\frac{1}{6} \rho_s d_s C_{p_s} \frac{dT_s}{dt} = h(T-T_s) - \sigma e_s T_s^4 \qquad (5.11)$$

where C_{p_s} = heat capacity of solid particle,

T_s = temperature of solid,

T = temperature of plasma,

h = heat transfer coefficient,

σ = Stefan-Boltzmann constant,

e_s = emissivity of solid particle.

The assumption is made that vaporization does not occur until the particle reaches the temperature for dissociation to AlO and O. As a result, no mass is lost during this time and a constant particle diameter can be used. The heat capacity of the solid varies little with temperature[27] so an average value is assumed. A constant emissivity is estimated because sufficient data were not available. At all times, the temperature throughout the particle is assumed to be equal to its surface temperature.

Vaporization of the solid particle to AlO and O is described by the combined heat and mass balance equation:

$$-\frac{1}{2}\Delta H_r^\circ \rho_s \frac{d(d_s)}{dt} = h(T-T_s) - \sigma e_s T_s^4 \qquad (5.12)$$

where ΔH_r° = heat of reaction for dissociation to Al and O (since the AlO initially formed quickly dissociates to Al and O). Assumptions are that the temperature of the solid remains constant during the dissociation, which proceeds uniformly. The heat transfer coefficient used in Equations (5.11) and (5.12) is:[8]

$$h = \frac{2k_f}{d_s} + 0.6\, R_{ef}^{0.5}\, P_{rf}^{0.3} \qquad (5.13)$$

where k_f = thermal conductivity of gas evaluated at an average temperature in the boundary layer around a particle,

R_{ef} = Reynolds number at average boundary layer temperature,

P_{rf} = Prandtl number at same temperature.

The relative velocity of the particle is used in evaluating the Reynolds number.

The two terms on the right hand side of Equation (5.13) represent the conductive and convective contributions respectively. Engelke[33] used purely conductive heat transfer in his model while Chludzinski[15] observed that the heat transfer to his thermocouples was convective. But for a small particle in relative laminar flow in a plasma, both contributions are important. Thermal radiation effects from the plasma can be neglected.[15,80]

The average boundary layer temperature at which the gas properties are evaluated is that which corresponds to the reference enthalpy given by:

$$h_{ref} = 0.5(h_{\infty}-h_s) + h_s \qquad (5.14)$$

where h_s = gas enthalpy at particle surface temperature,

h_{∞} = gas enthalpy at bulk plasma temperature.

This reference enthalpy method is suggested by Eckert[30] for the case of a large temperature difference across the boundary layer. The argon specific heats and enthalpies used in Equations (5.13) and (5.14) are given by Drellishak, et al.,[28] and the thermal conductivities and viscosities are obtained from Sherman and Grey.[81]

6. SPECTROGRAPHIC TEMPERATURE MEASUREMENTS

6.1 Meaning of Temperature and Local Thermal Equilibrium

Consider an isolated gas assembly containing a large number of identical particles which possess kinetic energy. According to statistical mechanics, an equilibrium distribution of particle energies or velocities will be established. Temperature is inherently related to this distribution. With a Maxwell-Boltzmann distribution (or M.B. distribution), the temperature can be related to the most probable velocity of the particles. In particular, the most probable kinetic energy of a particle in the gas is equal to the product of the Boltzmann constant and the temperature. By this definition, if a temperature is assigned to a gas assembly, a M.B. distribution of energies exists. The converse is also true.

An ionized gas consists of a finite number of different particle assemblies corresponding to the classes of particles present. Each of these assemblies could conceivably have a different initial energy distribution (and hence temperature). The final conditions reached in an isolated set of such assemblies depends upon the nature of collisions and energy exchange between particles. If energy is exchanged only between similar particles, the attainment of "equilibrium" would find each assembly with a different temperature. The other possibility would have all particles exchanging energy. In this case there is a unique final distribution for all the particles and the system has a single temperature. In such a system, the particles are in thermal equilibrium.

These isolated systems are actually nonexistent and energy exchange with the surroundings must be considered. Normally this additional exchange results in a directional flow of energy. But if a section of the assembly contains enough particles for equilibrium to exist, and the energy being transferred is much smaller than the total energy in the section, a local M.B. distribution can be obtained. In other words, collisions between particles not directly associated with energy transfer to the surroundings will predominate and maintain the distribution in the section. If the total assembly consists of such sections having local M.B. distributions and temperatures, it is in local thermal equilibrium (LTE). In practice, the temperature variation is considered to be continuous with the temperature at a point defining the local distribution. According to Chludzinski,[15] LTE exists in a radio frequency generated, induction-coupled argon plasma.

6.2 Relationship between Temperature and Atomic Line Intensity

In a plasma consisting of atoms, ions and electrons, all particles have translational energy, atoms and ions can possess electronic excitation energy and ions have ionization energy. Electronic excitation occurs in an atom when energy gained by collision causes an orbital electron of the atom to make a transition to an orbit of higher energy. If this electron in the higher energy state then makes a spontaneous transition to a lower energy level, a photon of light is emitted. The energy of this photon is equal to the difference in the energies of the upper and lower levels. The rate of these downward transitions depends upon a constant known as Einstein's probability of spontaneous transition.

The frequency of the emitted photons is:

$$\nu_{nm} = (E_n - E_m)/h \tag{6.1}$$

and the radiation intensity is:

$$I_{nm} = \frac{1}{4\pi} Lh \nu_{nm} A_{nm} N_n \tag{6.2}$$

where A_{nm} = Einstein's spontaneous transition probability for transition from n to m,

E_n, E_m = energies of upper level n and lower level m respectively, with respect to ground level,

h = Planck's constant,

ν_{nm} = frequency of emitted photon,

I_{nm} = radiant intensity (energy emitted per unit time per unit area per steradian),

L = path length through source,

N_n = number density of atoms with an electron in excited state n.

According to statistical mechanics, for an equilibrium system with a M.B. distribution, the concentration of excited atoms in state n is:

$$N_n = N_0 \frac{g_n}{g_0} \frac{1}{Q} \exp(-E_n/kT) \tag{6.3}$$

where N_0 = concentration of atoms in ground state,

g_n, g_0 = statistical weights of atoms in state n and ground state, respectively,

Q = electronic partition function,

k = Boltzmann constant,

T = absolute temperature.

Combining Equations (6.2) and (6.3) gives the relationship between temperature and atomic line intensity:

$$I_{nm} = \frac{1}{4\pi} Lh\ N_0\ \nu_{nm}\ A_{nm}\ \frac{g_n}{g_0}\ \frac{1}{Q} \exp(-E_n/kT) \qquad (6.4)$$

6.3 Determination of Argon Temperature

For argon atoms, the statistical weight of the ground electronic state is 1 and the electronic partition function is essentially 1.[82] Therefore, Equation (6.4) becomes:

$$I_{nm} = \frac{1}{4\pi} Lh\ N_0\ \nu_{nm}\ A_{nm}\ g_n \exp(-E_n/kT)\ . \qquad (6.5)$$

When LTE exists, the volume emission coefficient, ε_ℓ, for an optically thin spectral line of argon is:[9]

$$\varepsilon_\ell = \frac{h\ \nu_{nm}}{4\pi} N_0\ g_n\ A_{nm} \exp(-E_n/kT)\ . \qquad (6.6)$$

It follows from Equation (6.5) and (6.6) that the absolute line intensity averaged along the path length through the source is:

$$I_{nm} = \varepsilon_\ell L\ . \qquad (6.7)$$

The argon temperature can be determined from Equations (6.6) and (6.7) if the absolute intensity of a spectral line is measured and the transition probability of the line is known. This is known as the "single-line" method.

Since N_0 is temperature dependent, a graphical procedure is employed to determine the temperature. Using Drellishak's[28] values for N_0 and Gericke's[37] transition probabilities, the volume emission coefficient is calculated for various temperatures with Equation (6.6). Then ε_ℓ is plotted against T for the spectral lines of interest. By measuring I_{nm} and determining ε_ℓ from Equation (6.7), the temperature can readily be obtained. Figure 2 is such a plot for the optically thin 4158.59Å and 4259.36Å Ar_I lines.

6.4 Determination of Aluminum Temperature

Although local thermal equilibrium exists throughout an argon induction plasma, aluminum atoms introduced into the plasma by vaporization of alumina are not necessarily at the same temperature as the argon. Aluminum is formed from AlO dissociation at about 4400°K and cannot instantaneously reach the plasma temperature. In addition, the alumina vaporization occurs continuously along the reactor. So a steady stream of low temperature aluminum atoms is being introduced into the plasma at a given point in the reactor. Aluminum is also more easily ionized than argon, so that Al atoms are less likely to reach the higher kinetic energy levels. As a result, the average temperature of the Al atoms is lower than the argon plasma temperature.

The determination of the aluminum temperature is done by the "multi-line" method. Equation (6.4) is written for an unspecified line as:

$$I = K\nu gA \exp(-E/kT) \qquad (6.6)$$

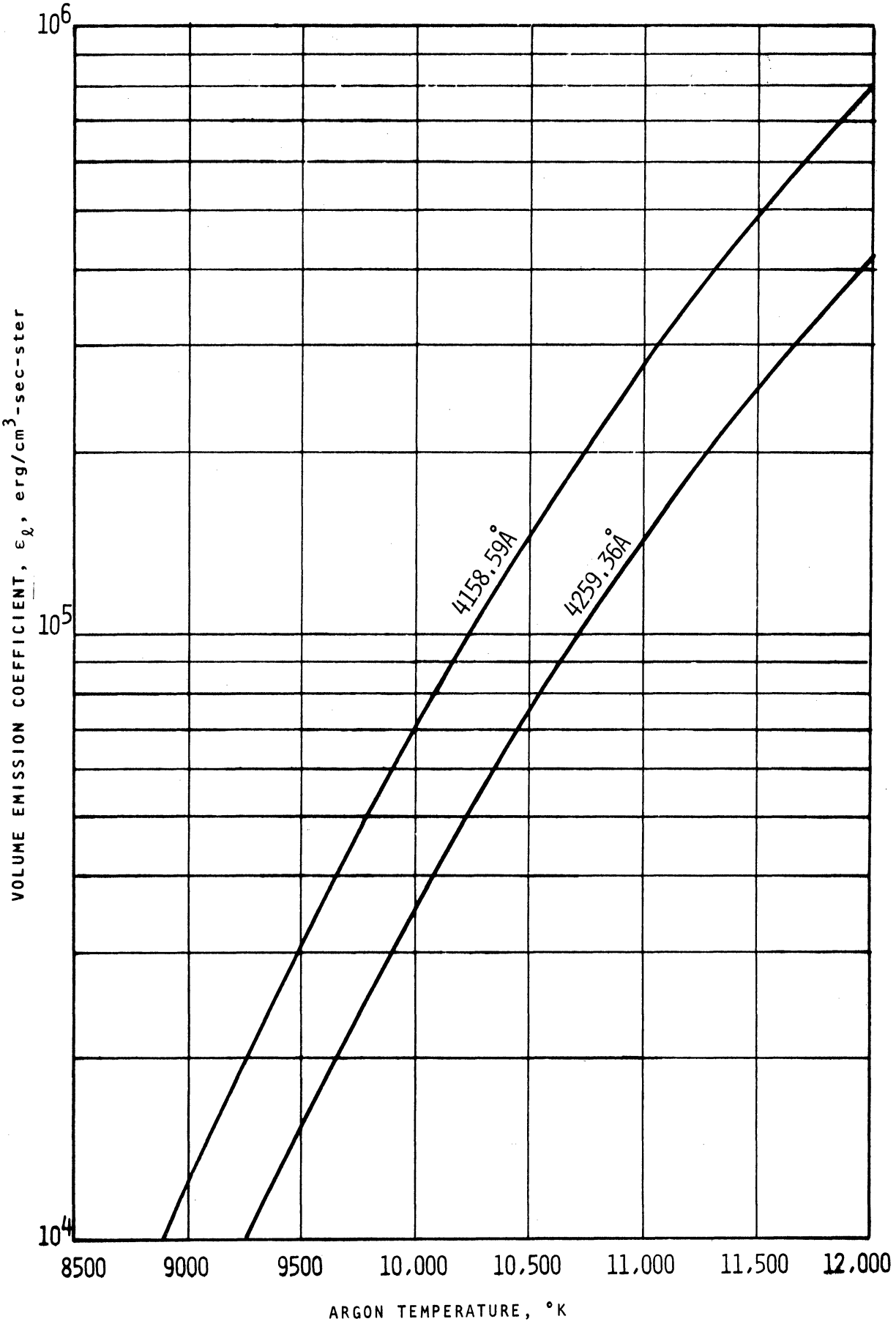

Figure 2. Argon Temperature from Volume Emission Coefficient.

where $K = LhN_0/4\pi g_0 Q$. (6.7)

Taking logarithms in Equation (6.6) gives:

$$\ell n(I/\nu gA) - \ell nK = - E/kT \ . \quad (6.8)$$

Since K does not depend on E, a plot of $\ell n(I/\nu gA)$ versus E for lines with different upper energy levels yields a straight line of slope $-1/kT$.

This relative method for temperature determination is necessary because of the build-up of aluminum and unvaporized alumina on the reactor wall during a run. The argon temperature, on the other hand, could be determined in the absence of alumina. The transition probabilities used in this work are those given by Corliss and Bozman,[21] although their value for the 3082.15Å Al_I line is contested by Dickerman and Deuel.[26] This is necessary because Corliss and Bozman's set is the only complete one available.

In addition to uncertainties in transition probabilities, Dickerman and Deuel found that self-absorption is invariably present in spectral lines of Al. Since self-absorption intensifies the line, and a 20 percent error in the intensity causes a 29 percent error in the temperature,[82] this method is not particularly accurate. As mentioned above, however, it is the only method available. The wavelengths, upper energy levels and transition probabilities for the Al_I lines used in this work are presented in Table I.

TABLE I

UPPER ENERGY LEVELS AND TRANSITION PROBABILITIES FOR Al_I LINES

Wavelength Å	Energy Level ev	gA 10^8/sec
3082.15	4.0214	2.7
3092.71	4.0217	5.5
3944.03	3.1427	0.66
3961.53	3.1427	1.3

7. ANALYTICAL METHODS

7.1 Bromate Method for Aluminum Determination

The bromate method is the standard volumetric procedure for determination of aluminum. The method can be accurate to within one percent for milligram amounts of aluminum. Interference is encountered when iron or titanium is also present, but these impurities can be removed prior to the aluminum determination.[62,63]

Using samples containing Al^{+3} in acid solution, the procedure followed in this work involves five main steps: (1) precipitation of aluminum quinolate from a solution of Al^{+3} and 8-quinolinol; (2) filtration of the precipitate and its dissolution in acid, forming 8-quinolinol; (3) bromination of the 8-quinolinol with a bromate-bromide solution; (4) reduction of the excess bromate with iodide, forming iodine; and (5) determination of the iodine with thiosulfate using a starch indicator. The precipitation of aluminum quinolate by 8-quinolinol is:

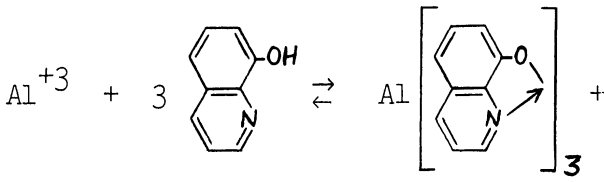

(7.1)

and the reverse reaction is the dissolution of the quinolate. The 8-quinolinol formed by dissolving the quinolate is then brominated by:

$$6H^+ + 5Br^- + BrO_3^- \rightleftarrows 3H_2O + 3Br_2 \qquad (7.2)$$

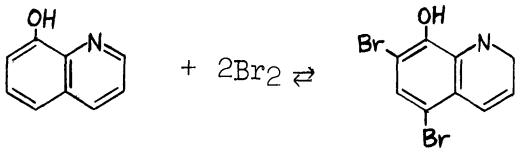

(7.3)

After the bromination reaction has reached completion, the excess bromine (obtained from the excess bromate by Equation (7.2)) is reduced:

$$Br_2 + 2I^- \rightleftarrows 2Br^- + I_2 \qquad (7.4)$$

This iodine is then reduced with thiosulfate by:

$$I_2 + 2S_2O_3^{=} \rightleftarrows 2I^- + S_4O_6^{=} \ . \qquad (7.5)$$

If a known volume of bromate is used, the excess is determined by the amount of thiosulfate required. Thus the amount of bromate which reacted with the 8-quinolinol is obtained. With 0.1 N BrO_3^- (0.1/6 molar) it can be seen from Equations (7.1), (7.2) and (7.3) that 1 ml of 0.1 N BrO_3^- (which reacts with 8-quinolinol) corresponds to 0.22483 mg aluminum.

7.2 X-Ray Diffraction

Since x-ray diffraction was used for an analysis of the reactant alumina and for the identification of the reduction products, its principles are briefly discussed. A thorough treatment is given in Cullity.[23]

Diffraction occurs when electromagnetic waves encounter a set of regularly spaced objects and the wavelength of the waves are of the same order of magnitude as the distance between the scattering objects. Such is the situation when x-rays are directed onto a crystal composed of regularly spaced atoms. The diffraction of a monochromatic beam of x-rays is governed by the Bragg law:

$$\lambda = 2d \sin \theta \qquad (7.6)$$

where λ = wavelength of x-rays,

d = spacing between crystal planes,

2θ = angle between diffracted beam and transmitted beam.

By using x-rays of known wavelength and continuously varying θ, it is possible to determine the spacing of the various planes in the crystal causing diffraction. This is done with an x-ray diffractometer, which can be set up to record the diffracted lines. If d is obtained for the three most intense lines of a given substance, then it can be identified with the help of the ASTM powder data file.[84] In this manner, it is possible to determine compounds and uncombined elements present in the sample and their phases.

7.3 X-Ray Fluorescence

X-ray fluorescence, which was also used in the analysis of the reactant alumina, differs somewhat from x-ray diffraction. In fluorescent analysis, the sample is bombarded with x-rays of sufficient energy that each element of the substance emits a characteristic line spectrum. This spectrum is analyzed in an x-ray spectrometer by diffracting the radiation with a crystal of known d spacing. If θ is determined, then the wavelengths of the characteristic lines can be calculated from Equation (7.6) and the elements can be identified, but the state of their chemical combination is not obtained by this method.

7.4 Optical Spectroscopy

The radiation emitted by a plasma or any other form of arc or spark discharge can be analyzed by means of optical spectroscopy. As with fluorescence, the spectrum emitted by an element or molecule is characteristic of the emitter. If the radiation from the discharge is passed through a prism or diffraction grating, the total spectrum is spread out and can be detected and recorded either photographically or with phototubes. Then if the spectrum can be separated into the spectra of the various emitting elements and molecules, these emitters can be identified with the help of the proper table of wavelengths.[50,56,72,78,79]

8. EXPERIMENTAL APPARATUS

8.1 General

The experimental system used in this investigation consisted of a plasma reactor, a radio frequency generator, a powder feed unit, gas delivery and cooling water systems, a safety interlock system, an exhaust fan and hood, and an optical spectrograph. This experimental setup is shown schematically in Figure 3. In addition, quench probes, x-ray sample probes, and equipment for plate development and analysis, x-ray analysis and wet chemical analysis were used.

8.2 Plasma Reactor

The radio frequency, induction-coupled plasmas were generated and contained in the reactor diagrammed in Figure 4. This plasma reactor consisted of a water-cooled quartz tube held in a brass distribution head. Argon was fed into the reactor through an axial entry port at the top of the head and through two 1/32 inch diameter tangential ports in the head. The use of tangential feed imparted a vortex motion to the gas, centrifuging the hotter atoms to the center and keeping the inside quartz wall relatively cool. The innermost quartz tube maintained the axial and tangential flows until just above the induction coil, where the plasma region began.

Argon was also introduced axially through the powder feed tube, which was a 12 inch long, 0.125 inch O.D., 0.094 inch I.D. alumina tube. The purpose of the first-mentioned axial gas stream was to provide a sheath for the powder as it entered the plasma with the carrier gas. This helped to keep the solids on the centerline of the plasma. The

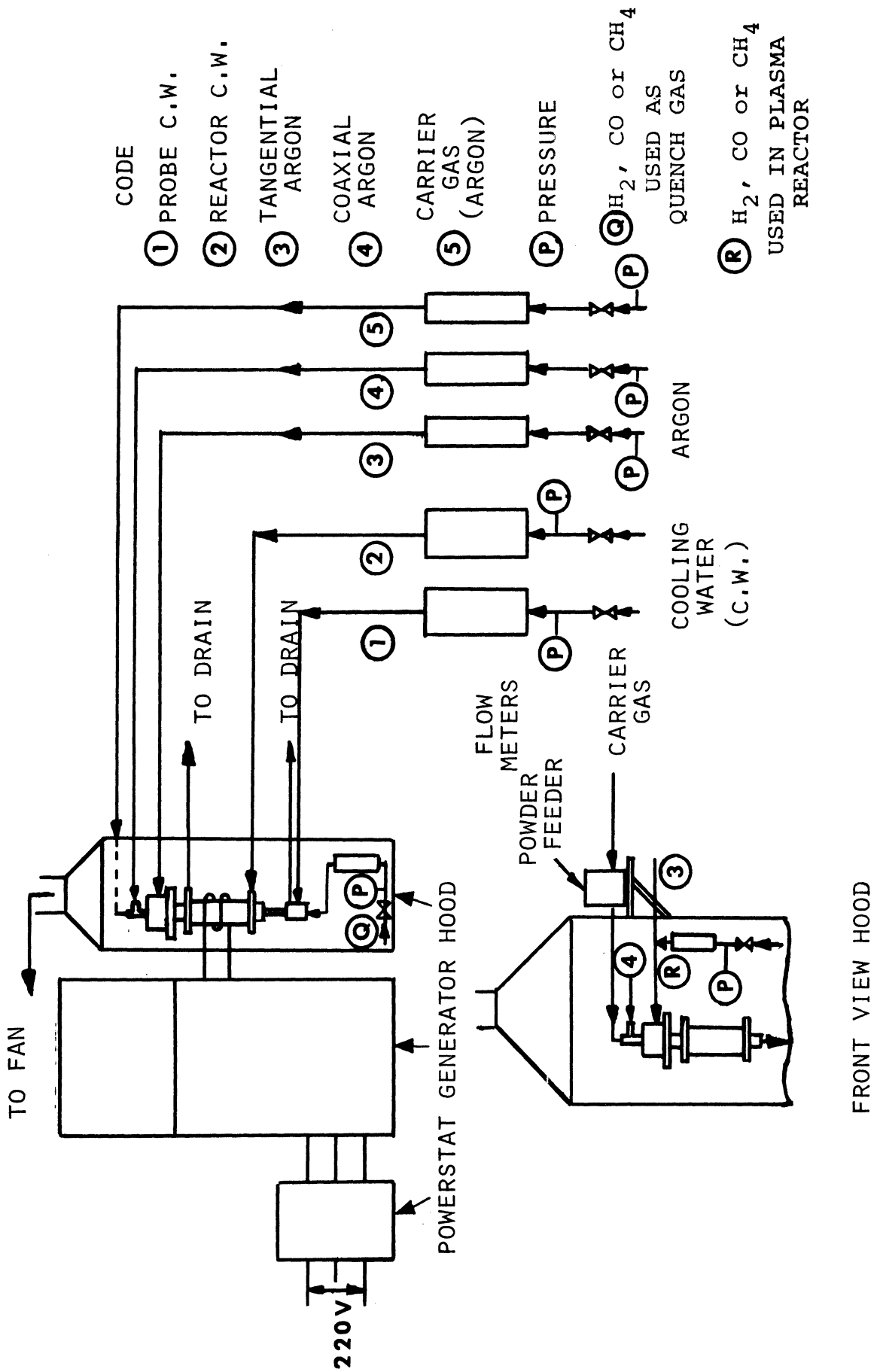

Figure 3. Schematic Diagram of Experimental System.

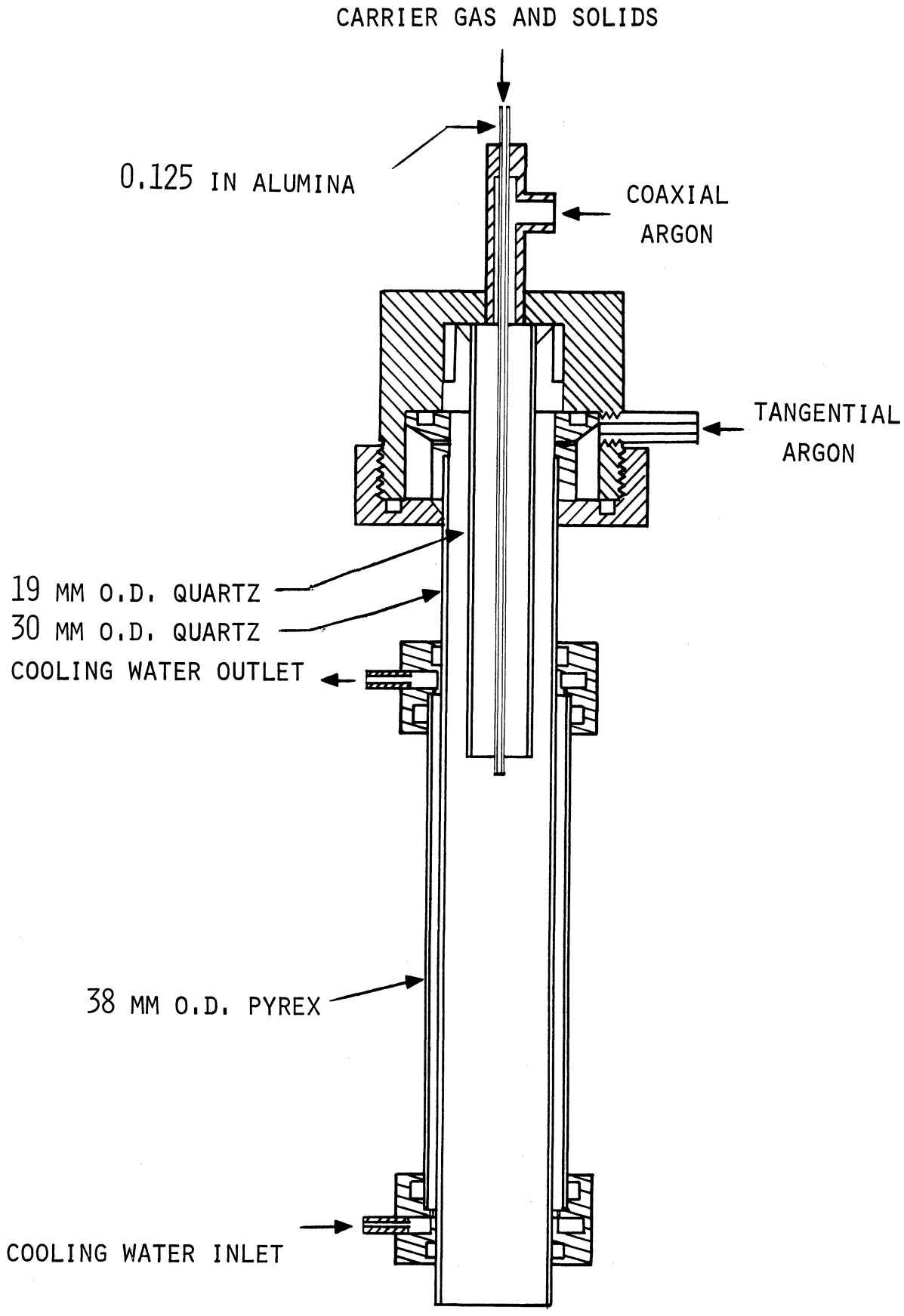

Figure 4. Induction-Coupled Plasma Reactor.

majority of the plasma gas was introduced tangentially and whenever H_2, CO or CH_4 was used in the plasma, they were introduced with the tangential argon.

8.3 Power Supply and Auxiliary Equipment

The radio frequency power for generating and maintaining the plasma was provided by a 23.5 KVA, 3 megacycle Lepel generator, Model T-10-3-3MC. By passing the r.f. current through a five turn induction coil, a 3 mc alternating electromagnetic field was produced and electrodeless discharge could be obtained. With this generator, a maximum power input to the plasma of about 10 kw was attainable. The original thyratron power control for the generator had been eliminated and replaced with a three phase powerstat on the primary side of the power transformer. This had been done to reduce the ripple of the r.f. power. The plasma column was initiated with the high voltage discharge of a tesla coil, which partially ionized the gas.

Feeding of alumina into the plasma was effected with a Plasmadyne Oscillating Powder Feed System. In operation, the powder hopper was vibrated by a variable amplitude oscillator to prevent packing and the argon carrier gas was passed through the bottom of the hopper. Powder was entrained in the carrier gas by way of a venturi pickup. The top of the hopper was sealed off during operation to prevent loss of gas pressure in the container.

The gases used in the plasma and for quenching were supplied through calibrated Fischer-Porter Tri-flat rotameters. The gases were delivered to the rotameters at a pressure of 30 psig and entered the

reactor at atmospheric pressure. Cooling of the reactor and the quench probes was effected with tap water, which was supplied at line pressure. The reactor was protected against insufficient tangential gas and cooling water flow by safety interlocks, which would shut off the power.

Since H_2, CO and CH_4 were used in this study, the reactor was enclosed in a 2 by 4 by 7 foot plywood hood, open on one side. Air was sucked through the hood at the rate of 1210 cfm by a Buffalo Forge Company exhaust fan driven by a 5 hp motor. Spark proof construction was used for the fan shaft and wheel.

8.4 Spectrographic Equipment

A 3.4 meter focal length Ebert Mark IV stigmatic plane grating spectrograph manufactured by the Jarrell-Ash Company was used to analyze the radiation from the plasma. The spectrograph was equipped with a grating ruled with 15,000 lines/in giving a first order linear dispersion of 5.1 Å/mm at the focal plane over a useful range of 2100 to 7500 Å. The entrance slit of the spectrograph could be adjusted in width from 4 to 400μ and in height from 1 to 15 mm.

The Jarrell-Ash Number 18-022 scanning and condensing system could be used to scan and focus selected areas of an extended source onto the spectrographic slit. Seven front surface mirrors and two quartz-lithium fluoride acromatic doublet lenses automatically maintained focus and alignment with the optical axis of the spectrograph. A 1.72 to 1 image reduction between the plasma and the spectrographic slit was caused by the lenses.

Depending upon the application of the spectrograph, the spectra were either recorded on two 4 by 10 inch Kodak SA1 Spectrum Analysis Plates or by an RCA 1P28 multiplier phototube located at the center of the focal plane (direct read-out). By placing the two plates end to end, a total first order range of 2400 Å was recorded during a single exposure. The phototube was operated with a supply voltage of 1000 volts dc obtained from a Furst Electronics (No. 710-PR) dc power supply with a continuously adjustable voltage output from 0 to 1500 volts. The current output of the phototube was passed through a variable precision resistor and the resulting voltage amplified by a variable range Leeds and Northrup (No. 9835-A) stabilized dc μv amplifier. The amplifier output (0-10 mv) was recorded with a Leeds and Northrup Speedomax H strip chart recorder.

Horizontal scanning of the plasma (perpendicular to the axis of symmetry) was done by turning a screw drive which moved the mirror assembly. Vertical scans (parallel to the plasma axis) were made by pivoting a mirror. The spectrum at a given position in the plasma could be scanned (when direct read-out was used) with a sine bar wavelength drive (Jarrell-Ash No. 70-005), which rotates the grating so that the wavelength seen by the center of the focal plane corresponds to the wavelength indicated on a counter. Twelve scan rates, ranging from 1 to 500 Å/min were available.

8.5 Quench Probes

The quench probes were used both to augment the recovery of product by collection on its outer wall and to introduce quench gases

countercurrent to the plasma flow. To meet this dual need, a water-cooled probe consisting of three concentric stainless tubes was used (see Figure 5). Three different probes were used, with outer tube outside diameters of 0.148 inch, 0.250 inch and 0.375 inch. The two larger probes had stainless tips heliarced to the tubing and the smallest probe had a copper tip silver soldered to the probe.

8.6 X-Ray Sample Probe

The x-ray sample probe was designed to collect product samples suitable for x-ray diffraction analysis. X-ray samples could not be prepared in the usual way (grinding to -200 mesh and mixing into a matrix of vaseline) because of the highly pyrophoric nature of some of the product. The sample probe, shown in Figure 6, was a water-cooled, 0.250 inch O.D. copper tube. A small cup was made on the end by setting a thin copper disc inside the tubing and silver soldering it in place. After collection of a sample, the cup was cut off and a new one made for the next run.

8.7 Plate Development and Analysis Equipment

The two 4 by 10 inch Spectrum Analysis Plates used for a given set of runs were developed singly in a temperature controlled tank. The developer and fixer temperatures were held to within $\pm$ 0.2°F. During the developing and fixing, continuous agitation was applied to the fluid in the trays. The plates were analyzed by scanning the spectra with a Leeds and Northrup Recording Microphotometer (No. 6700-P-1) in conjunction with a Leeds and Northrup Speedomas G Logarithmic strip chart recorder.

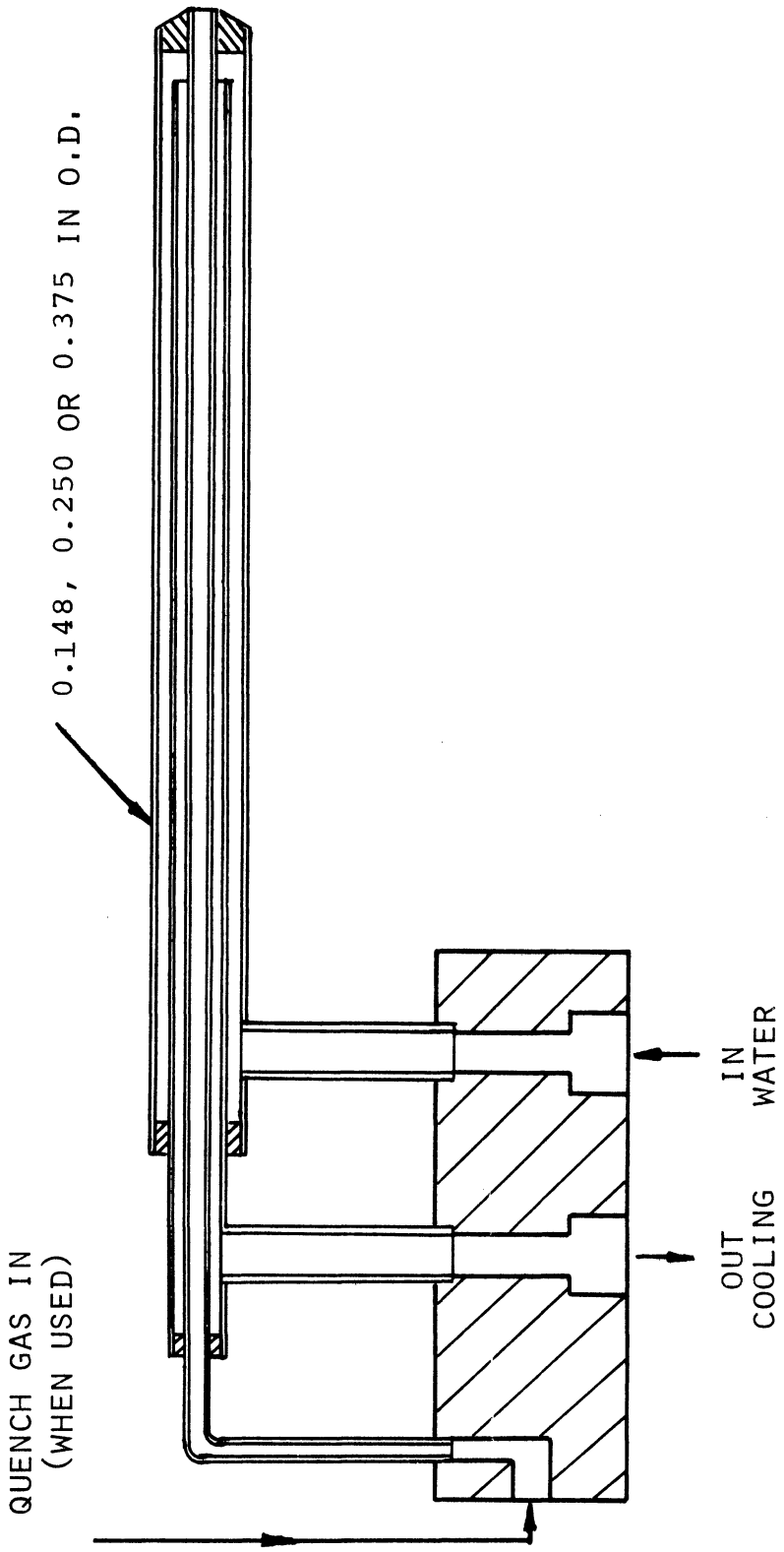

Figure 5. Quench Probe.

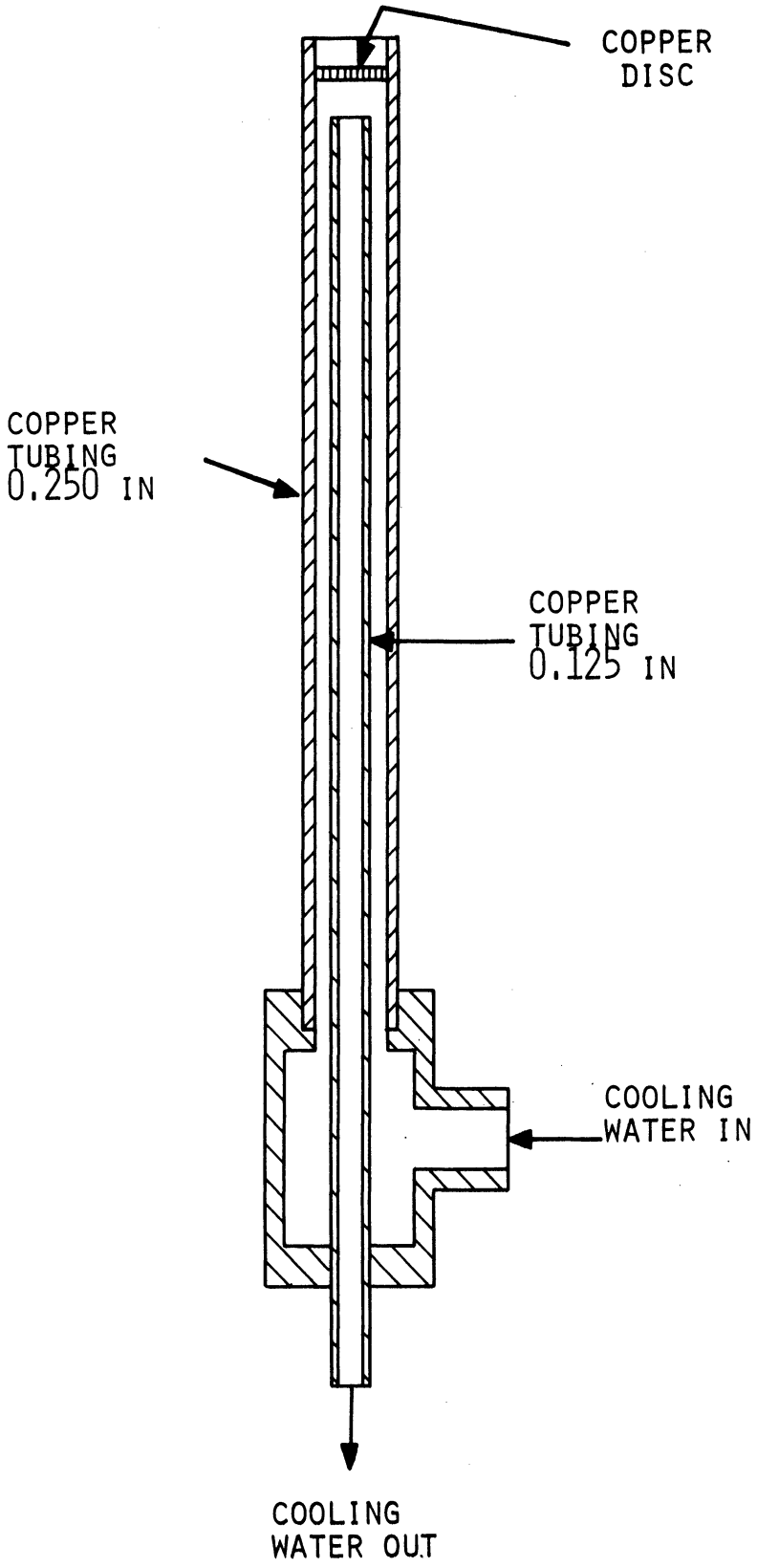

Figure 6. X-Ray Sample Probe.

8.8 X-Ray and Wet Chemical Analysis Equipment

The x-ray diffraction analyses were done with a Norelco Diffractometer (Type 42202) using a copper target. A Norelco Universal Vacuum X-ray Spectrograph (Type 52530) with a chromium target and either a LiF or EDDT crystal was used for the fluorescent analyses. The output from the diffractometer and spectrograph was recorded with a Minneapolis-Honeywell strip chart recorder.

The quinolate precipitations were performed in 50 ml erlenmeyer flasks and the precipitates were filtered out with a sintered glass funnel, using vacuum. The solution was cooled to 60°C, prior to the filtration, in a constant temperature bath. The dissolution of the precipitate and all subsequent operations occurred in a 250 ml iodine determination flask. All weighings of less than 200 gm were performed with a RIGHT-A-WEIGH balance manufactured by William Ainsworth and Sons, Incorporated. This balance is accurate to $\pm$ 0.2 mg. Quantities of over 200 gm were weighed on a Mettler (Tara 0-2000 gm) balance, which is accurate to $\pm$ 0.5 gm.

9. EXPERIMENTAL PROCEDURES

9.1 Start-Up and Safety Procedures

After supplying cooling water to the generator and throwing a line power switch, the oscillator filament was actuated and allowed to warm up until the plate ready light began to glow. Then the argon (including carrier gas) and cooling water flows were initiated. Power was supplied to the plate, the powerstat set on 50 and the grid current adjusted to 10 percent of the plate current with the grid control. The powerstat was set on 70 and the high voltage from the tesla coil was applied to the argon above the induction coil to partially ionize the gas and create a discharge. If a stable discharge was not obtained, the powerstat reading was increased and the tesla coil treatment repeated until the discharge persisted. By slowly increasing the powerstat reading, the plasma was obtained. The plasma intensity was then maximized by readjusting the grid current to 10 percent of the plate current with the grid control. The desired operating conditions were set by proper balancing of the power and grid controls. Oxyacetylene welding goggles were worn whenever the plasma was viewed directly and warning lights, which had been installed at the laboratory entrances, were on during all plasma operations.

When the reducing gases, H_2, CO or CH_4 were used, the exhaust fan was turned on and the feed line for the gas was flushed with helium. It was determined (by conversing with The University of Michigan Environmental Health personnel) that an exhaust rate of 1210 cfm of air was adequate protection against a maximum possible H_2 usage

of 1 cfm. The plasma was initiated and optimized with argon as described above. If the reducing gas was to be used in the plasma itself, the gas was slowly bled into the plasma with the tangential argon while the power and grid controls were constantly adjusted. When the desired reducing gas flow rate was reached, the power level for the run was set and the grid current-plate current ratio balanced.

The use of H_2, CO or CH_4 as a quench gas did not affect the generator operating conditions since the gas did not pass through the induction coil. Therefore, much higher flow rates of the reducing gases were possible. After the argon plasma was started and the operating conditions were set, the quench probe was positioned in the plasma with a vertical traversing mechanism to be about 3/4 inch below the induction coil, as shown in Figure 7. This could not be done prior to the plasma start-up since the induction coil would couple to the probe instead of the argon and a plasma could not be obtained. When the probe position was properly set, the quench gas flow was initiated and brought to the desired level.

The correct aluminum oxide flow rate was attained by adjustment of the position of the venturi tube in the bottom of the hopper (a constant carrier gas flow rate was used). The powder pick-up arrangement is depicted in Figure 8. The powder flow rate was determined by weighing samples collected during a known time interval. This was done before and after each run. The oxide was not introduced into the reactor until the plasma had been established.

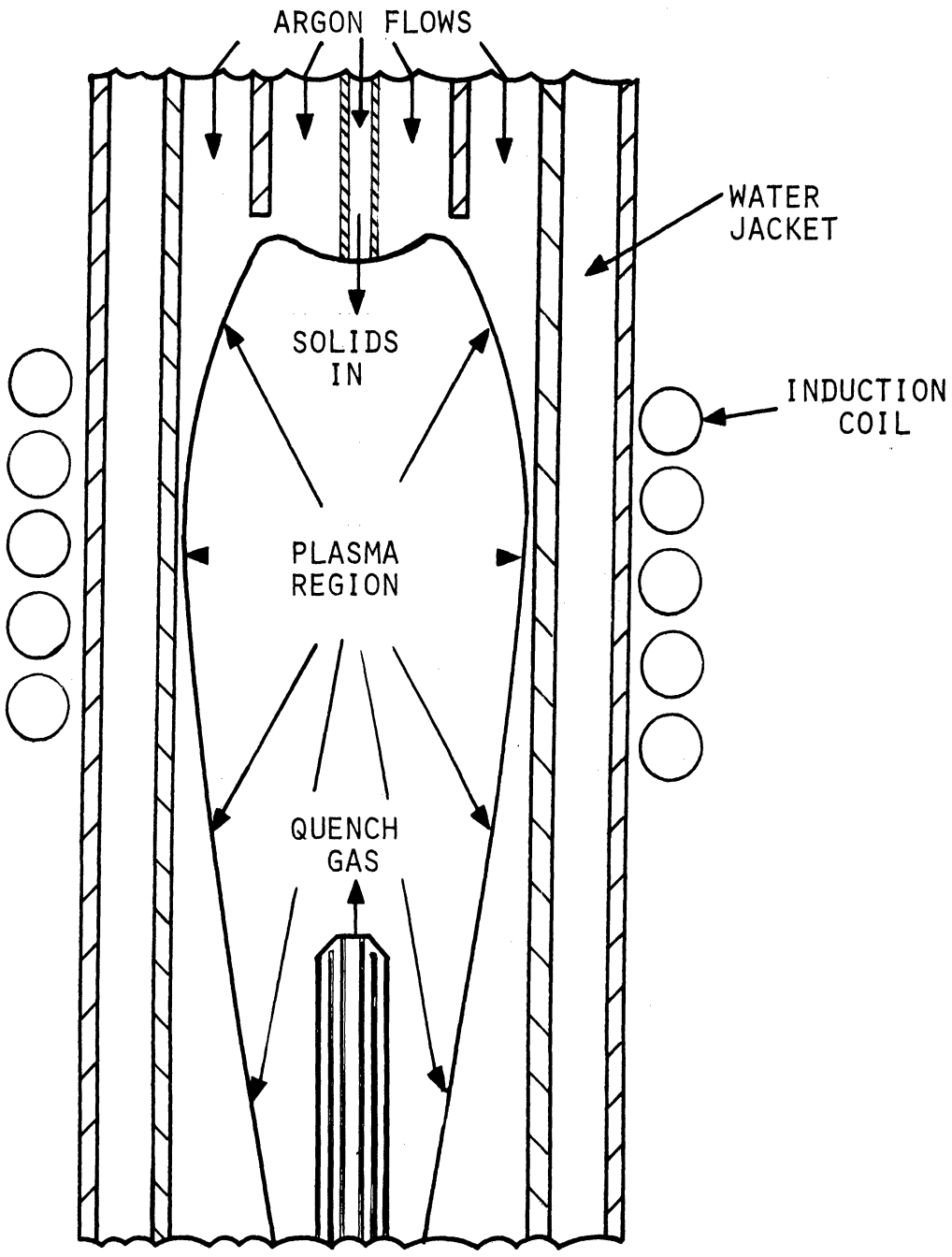

Figure 7. Position of Quench Probe in Reactor.

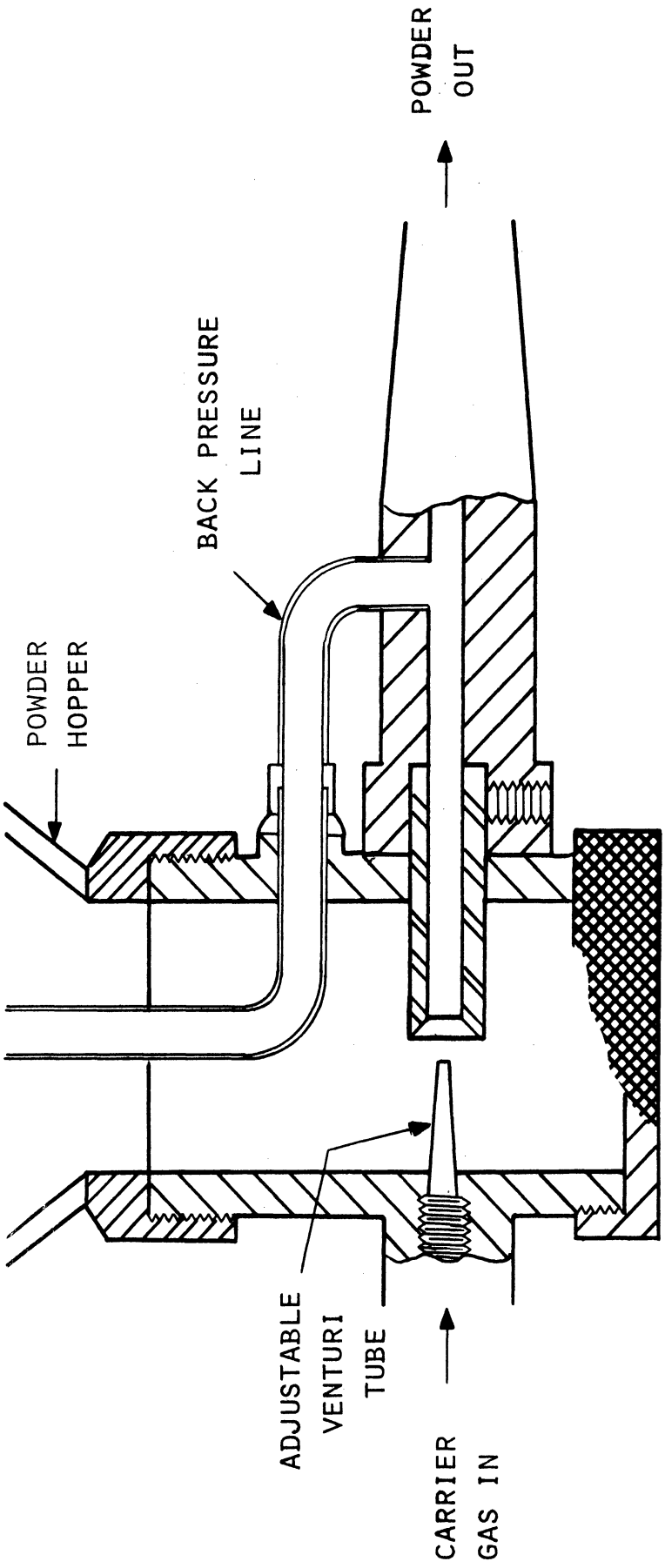

Figure 8. Powder Pick-up Arrangement in Bottom of Hopper.

9.2 Selection of Reactor Design

According to Marynowski,[68] when solids are fed into a plasma, it is desirable to use an induction coil with a reverse turn at the bottom in order to achieve axial stability of the plasma. Supposedly, the introduction of solids shifts the vertical position of the plasma. This is prevented by the reverse turn, which sets up a magnetic field in opposition to the plasma flow. This approach was tried in the initial experiments, but was found to be unsuitable. With a coil of five turns in one direction and one reverse turn, an arc between the reverse coil and the cooling water was invariably obtained during the start-up of the plasma. The result was breakage of the pyrex cooling water jacket. Since a glass reactor was necessary for the spectrographic studies, the above coil had to be abandoned. The coil was replaced by a simple five turn coil and axial stability problems were not encountered.

In an attempt to collect all of the reduction products, a brass product collector preceded by a water-cooled quench chamber was placed directly below the reactor. Although the chambers were supported from below, they put too much constraint on the quartz reactor. As a result, the reactor would break during a run. Since the brass chambers had to be discarded it was decided to forego total collection of the products. So the conversion was based upon the amount of material actually collected and quench probes were used to increase the recovery.

The third item of importance was the choice of an alumina powder feed tube. A water-cooled stainless feed tube, similar to the quench probes (see Figure 5), was first tried. In order to achieve

centerline feed of the solids into the plasma, however, the tube tip had to be placed about a half inch above the induction coil. This caused arcing from the coil to the tip and water leaks developed. The alumina tube was then tried and was found to be perfectly suitable. Even though the plasma region began at the end of the tube, melting did not occur.

9.3 Qualitative Analysis of Alumina

Since the aluminum oxide used in this investigation was not chemically pure, an analysis of the material was necessary. The presence of small impurities would not affect the alumina reduction but could interfere with the quantitative analysis for aluminum. A probable analysis of the alumina was supplied by the manufacturer (Carborundum Corporation) and it was checked by the methods discussed in this section.

X-ray diffraction, x-ray fluorescence, and optical spectroscopy were all used for the alumina analysis. A sample of aluminum oxide in a matrix of vaseline was analyzed with the diffractometer. The procedure was to scan the region from $2\theta = 15°$ to $80°$ (see Section 7.2) and identify the line spectrum as much as possible. Fluorescent analysis of alumina powder was similarly performed. The powder was placed in the spectrograph, a vacuum drawn and 2θ varied over a range large enough for identification of the elements present. Both LiF and EDDT cyrstals were used for the analysis. The x-ray tube power supply was operated at 35 KV and 15 ma for the diffraction and fluorescence studies.

Optical spectroscopy was used in two different experiments. In the first, alumina was fed into a plasma and various regions of the spectrum were scanned using direct read-out. Identification of the spectral lines constituted an analysis of the elements present in the alumina. For the other analysis, alumina was put in a hollow cup made in the end of the vertical electrode of a carbon arc lamp (Bausch and Lamb Optical Company, Automatic Arc Lamp, 5-10 amperes dc). The lamp was mounted on the optical bench of the spectrograph, an arc was struck and the spectrum recorded on a pair of SA1 plates. Analysis of the spectrum identified the elements present.

9.4 Analysis of Reaction Zones

The purpose of analyzing various sections of the plasma was to identify the aluminum containing species present. This was expected to provide significant information about the nature of the vaporization and quench processes. The analysis was performed with the optical spectrograph, using direct read-out, by scanning spectral regions of interest at various points in the plasma.

9.5 Identification of Product

The rigorous Group III qualitative chemical analysis given by McAlpine and Soule[69] was used to examine the product for the presence of Al, Fe and Cr. "Aluminon-reagent" (0.1 percent solution of ammonium aurin tricarboxylate) was the aluminum detector. Prior to this determination, the product was placed in half concentrated HCl to put the metals into solution.

It is conceivable that AlO or Al_2O might also form Al^{+3} in HCl and give a positive "aluminon" test. Since AlO and Al_2O were not ruled out as possible products, an x-ray diffraction analysis of the product was also made. Three product samples were obtained with the x-ray sample probe set directly in the plasma, using the vertical traversing mechanism (as in Figure 7). The samples were mounted linearly in a standard x-ray sample holder. The sample holder was rotated to give a maximum intensity for the α- Al_2O_3 line at $2\theta = 37.75°$. Then 2θ was varied continuously to give a spectrum of diffraction lines.

Samples collected in Ar-CO and Ar-CH_4 plasmas were also examined by diffraction analysis. This was done to see what effect the addition of carbon to the system had on the nature of the products.

9.6 Determination of Aluminum

The following procedure was followed to determine the amount of Al in a given product sample:

1. Put the product in half concentrated HCl (to dissolve the Al) and weigh the total. Use a weighed flask.
2. Allow the undissolved solids to settle and determine the density of the solution by pipetting off and weighing three 10 ml portions.
3. Pipette off most of the remaining solution and save.
4. Wash the solids, filter and weigh.
5. Take a known volume of the solution, precipitate the aluminum quinolate and cool to 60°C. Two samples were used for each run.

6. Filter the quinolate, dissolve in HCl and determine the Al by the bromate method.
7. Determine the volume of the total solution from steps 1, 2 and 4.

The Al density of the sample in step 5, multiplied by the total volume, was the total amount of Al in the product.

The method used for precipitation of aluminum quinolate[63] applies to solutions containing not more than 0.5 mg Al/ml. Tartaric acid equal to about five times the amount of Al present and 4 to 6 gm ammonium acetate were added to the solution. Bromocresol purple (8-10 drops) was added and the solution neutralized to the purple end point with half concentrated NH_4OH. An excess of 8-quinolinol (1 ml/3 mg Al) was added, the solution heated in a boiling water bath until a yellow precipitate was obtained and the mixture cooled to 60°C in a constant temperature bath.

The 60°C solution was filtered with moderate suction through a sintered glass funnel and the quinolate washed with 100 ml of cool water. The precipitate was dissolved in half concentrated HCl and dilute HCl was sucked through the frit and added to the volume.

The 8-quinolinol formed by dissolution of the aluminum quinolate in HCl was brominated with the $KBrO_3$-KBr solution. An excess of about 2-3 ml of the solution was added; the mixture stirred and allowed to react for 60 seconds. An excess of the 20 percent KI was added and the iodine titrated with thiosulfate to the starch end point. The starch was added just before the yellow iodine color disappeared to prevent

unfavorable side reactions. This method is discussed in greater detail by Kolthoff and Belcher.[63]

The effect of Fe and Ti in the product was investigated by removal of the impurities and determination of the Al . Kolthoff and Belcher[63] agree with Kodama[62] that Fe and Ti quinolates precipitate in the presence of sodium malonate in 5 to 10 percent acetic acid. Therefore a known volume of solution (see step 3 above) was neutralized with NH_4OH and glacial acetic acid added. Di sodium malonate (80 times that needed to complex the Al) was added, the solution diluted to give 5 to 10 percent acetic acid and 8-quinolinol added. The solution was boiled gently to precipitate the Fe and Ti quinolates, cooled to 60°C and filtered.

The filtrate was treated to form aluminum quinolate by addition of tartaric acid, ammonium acetate and dropwise addition of NH_4OH and 8-quinolinol. The precipitation was done in a boiling water bath. The amount of aluminum was then determined by the method outlined above. The Fe-Ti removal procedure was repeated with a pure Al^{+3} solution as a check.

9.7 Measurement of Argon Temperature

The argon temperature was measured at the power levels studied in this work, using a clear reactor of known transmittance (see Appendix IV). The 4158.59 and 4259.36 Å Ar_I lines were scanned at 10 Å/min and the outputs of the direct read-out from the optical spectrograph were integrated to give the absolute line intensities. The argon temperature was then determined as the average of the two values obtained

from Figure 2. Since radial temperature profiles exist in the plasma, the argon temperature obtained above represents an average along the diameter of the plasma.

9.8 Measurement of Aluminum Temperature

Aluminum temperatures were determined by the method discussed in Section 6.4 for most of the final experimental runs. The temperatures were measured at a point 1/2 inch below the coil on the centerline of the plasma and are an average for the plasma along the diameter. The spectra at this position were recorded on the SAl plates with the use of the optical spectrograph.

Line profiles were obtained for the 3082.15 Å, 3092.71 Å, 3944.03 Å, 3961.53 Å Al_I lines used in this work. The lines were scanned with the recording microphotometer to give profiles of silver density of the line recorded on the plate versus wavelength. These were converted to relative intensity versus wavelength by the calibration curves (see Appendix III). Integration of these profiles gave the absolute intensities of the four lines and the temperature followed from the "multi-line" method. The integration procedure is discussed in Appendix VI.

9.9 Study of Reaction Variables

The three variables that were studied in detail were the Al_2O_3 particle size, Al_2O_3 mass flow rate and power input to the plasma. This three variable investigation was preceded by an examination of the effect that build-up of solids on the reactor wall had on conversion of alumina. The purpose was to see if it would be necessary to limit the length of the runs.

The Al_2O_3 particle size and flow rate were varied at a constant power input level (the lowest power level of this work). Several flow rates were used for the smallest particle size to determine the shape of the flow rate versus conversion curve. This made it possible to use only three flow rates for the other two particle sizes and still cover roughly the same range of conversions. The effect of power input was determined by a single set of runs. Three power input levels were used at a constant Al_2O_3 flow rate and the smallest particle size.

The use of diatomic and polyatomic gases, viz. H_2, CO and CH_4, in a plasma requires considerably more power than argon alone. Since the range of reducing gas flow rates was restricted by the power capacity of the r.f. generator, it was decided to use a single run for each of the three gases. An intermediate Al_2O_3 flow rate and the smallest particle size were used for the runs. The argon flow rates were maintained constant for all of the runs discussed in this section.

9.10 Quench Methods

For the experiments covered in Section 9.9, the conversion of alumina to Al was based on the amount of product collected instead of the Al_2O_3 input flow rate. Water-cooled quench probes were then used to show that it would be possible to increase the recovery without lowering the conversion. The significance is that if a reactor were designed to recover nearly all of the product, the conversions obtained in this work would be maintained. This could be done, for example, with a water-cooled metallic reactor followed by a suitable

collection chamber. The probes were positioned directly in the plasma so that the tip was about 3/4 in below the coil (see Figure 7). This was done with a vertical traversing mechanism. Three probe sizes were tried and a single run was made with each, using the smallest Al_2O_3 particle size.

The effect of H_2, CO and CH_4 as quench gases was determined by introducing the gases through the 0.250 in O.D. quench probe counter-current to the plasma. The probe tip was an inch below the coil. Several H_2 flow rates and one each for CO and CH_4 were used.

10. EXPERIMENTAL RESULTS AND ANALYSIS

10.1 General

The scope of this work was outlined in Chapter 4 and discussed in greater detail in Chapter 9. The results of the experimental program are presented and analyzed in this chapter.

10.2 Qualitative Analysis of Alumina

The reactant aluminum oxide was analyzed by several qualitative techniques and the results compared with the probable composition supplied by the manufacturer (Carborundum Corporation). It was not possible to obtain a complete analysis by any one of the techniques employed, but the composite analysis was essentially complete. The results of the various analyses are presented in Table II and the composite analysis is compared with Carborundum's probable analysis in Table III.

TABLE II

ANALYSES OF REACTANT ALUMINUM OXIDE

1. X-ray Diffraction	2. X-ray Fluorescence	3. Optical Spectroscopy (a) Plasma	(b) Carbon Arc
α-Al_2O_3	Ti	Al	Al
	Fe	Ti	Ti
a few unidentified impurities	Zr	Fe	Fe
	Ca		Si

TABLE III

COMPARISON OF COMPOSITE ANALYSIS
WITH CARBORUNDUM'S PROBABLE ANALYSIS

Composite Analysis	Carborundum's Composition		
α-Al_2O_3	α-Al_2O_3	97.03	%
Ti	TiO_2	2.10	
Si	SiO_2	0.50	
Fe	Fe_2O_3	0.20	
Zr	ZrO_2	0.13	
	Na_2O	0.02	
Ca	MgO+CaO	0.02	
		100.00	%

X-ray fluorescent and optical spectroscopic analyses identify only the elements present in a sample and not the state of their chemical combination. Diffraction analysis determines the compounds present but requires at least three diffraction lines for a positive identification of a substance. Thus it is not very suitable for impurities present in small amounts. None of the analytical techniques used are particularly sensitive to oxygen or small concentrations of Mg or Na . Consequently, the composite analysis is in substantial agreement with Carborundum's probable composition and the latter can be accepted as true.

The presence of TiO_2, Fe_2O_3, ZrO_2 and SiO_2 in the reactant alumina indicated that Ti, Fe, Zr and Si would be possible contaminants in any reduction product. Therefore, the effect that their presence would have on a quantitative analysis for Al was determined. The result of this investigation is given in Section 10.5.

10.3 Analysis of Reaction Zones

The aluminum containing species were identified at various points in the argon plasma and tail flame by using the direct read-out of the spectrograph. As is shown in Figure 9, the plasma core consisted only of atomic and ionic species. This hot core was surrounded by a thin region containing AlO and Al . Both AlO and Al were also detected throughout the cooler tail flame of the plasma. Figure 10 shows typical Al_I lines in the plasma core and their intensities relative to nearby Ti_{II} lines. The presence of Ti_{II} lines throughout the spectrum instead of Ti_I is explained by the greater relative intensities of the Ti_{II} lines. The Fe_I lines were also much weaker than Ti_{II} lines although the former were definitely obtained.

The 4850 Å, $^2\Sigma$- $^2\Sigma$ band system of AlO was observed in the tail flame and is partially presented in Figure 11. It was impossible to discern if Al_2O was also present anywhere in the plasma since Al_2O spectra have not been reported in the literature. However, some negative inference can be drawn from the absence of extraneous band structure, which could be attributed to Al_2O , throughout the spectral regions scanned.

Although AlO was not observed in the hot plasma core, its presence in the cooler regions of the argon plasma supports the contention

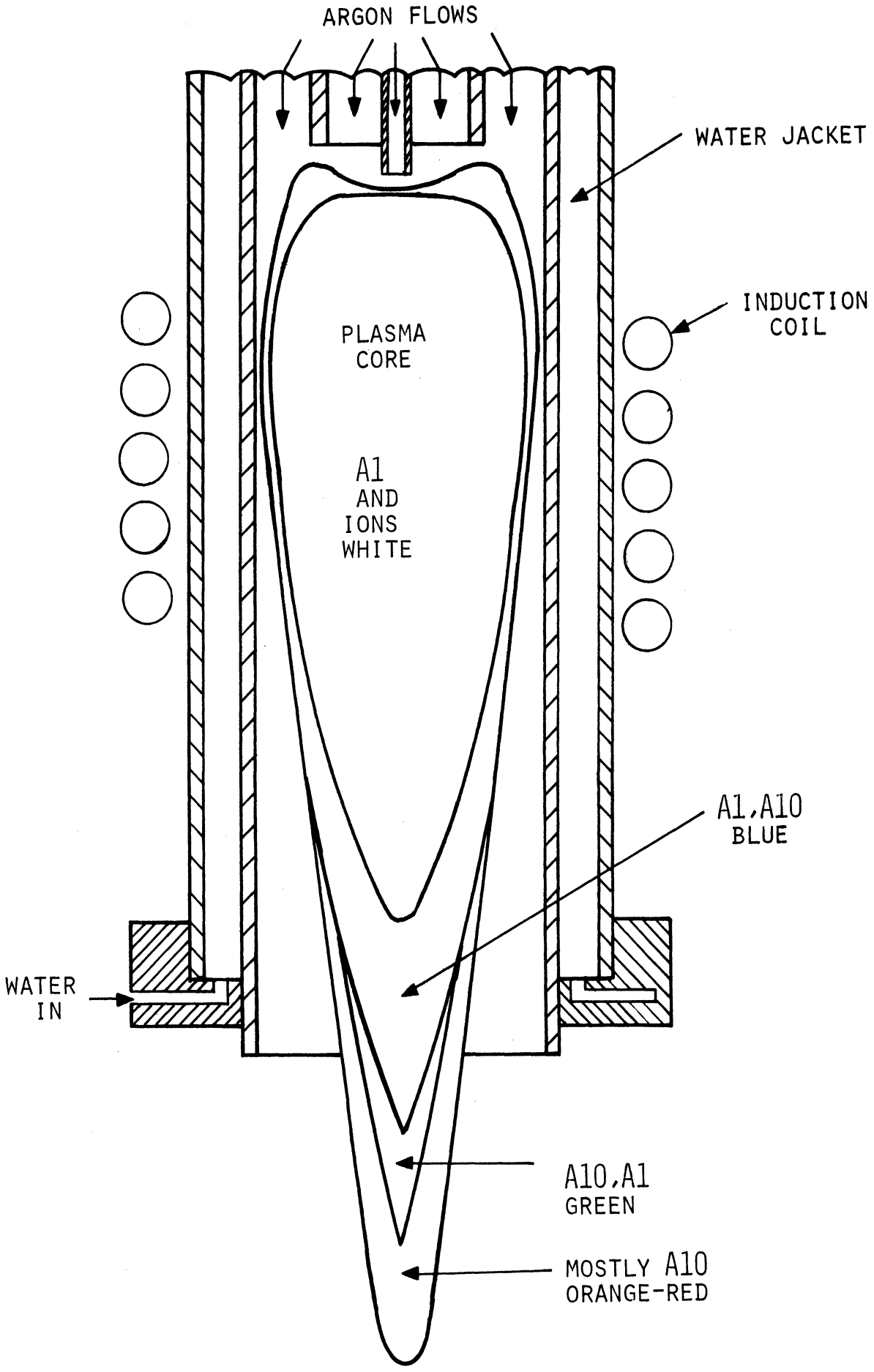

Figure 9. Composition of the Sections of the Plasma.

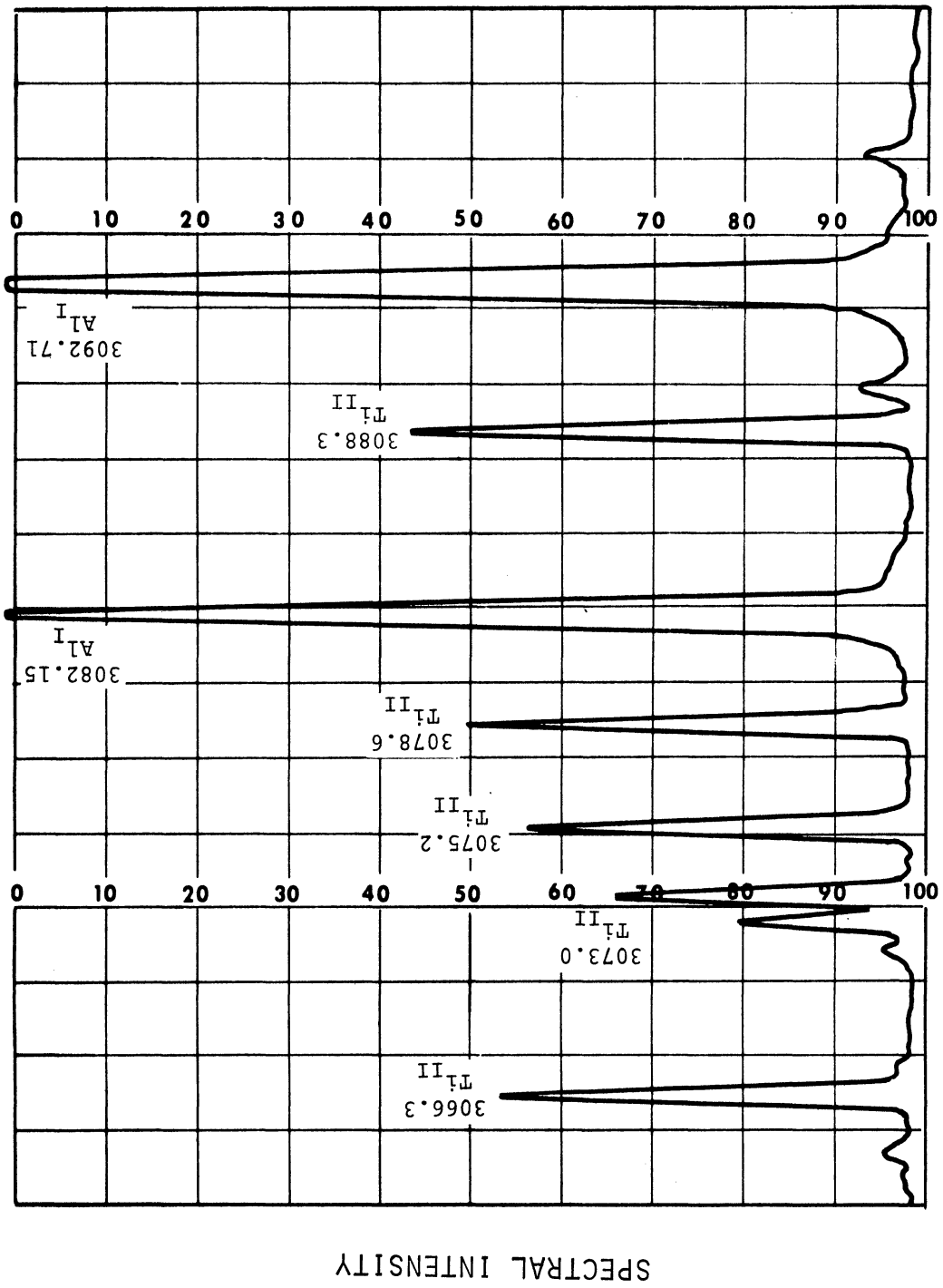

Figure 10. Typical 3082.15 and 3092.71 Å Al_I Lines in the Core of an Argon Plasma.

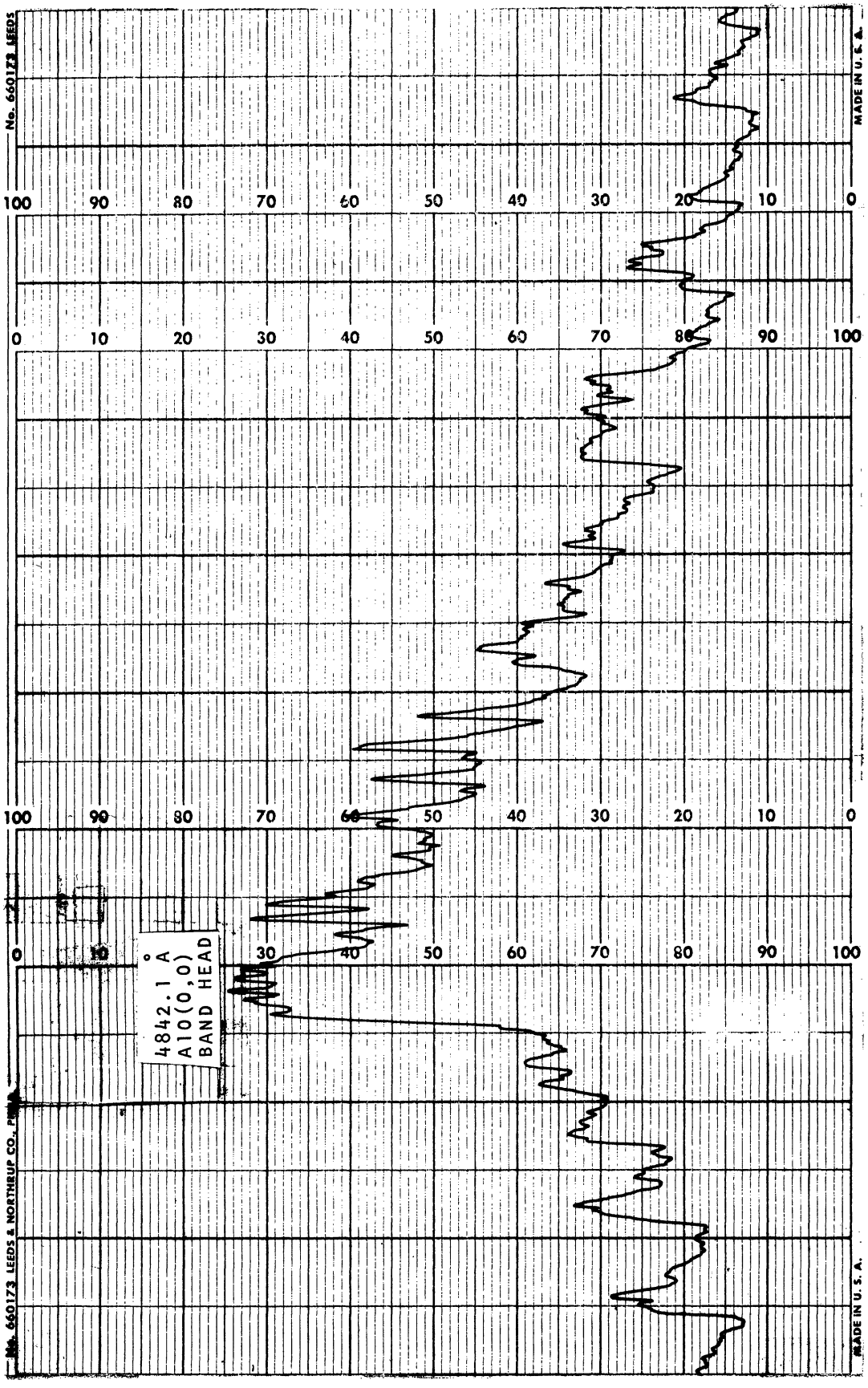

Figure 11. The 4842 Å AlO(0,0) Band of the 4850 Å $^2\Sigma - ^2\Sigma$ Band System of AlO Observed in the Tail Flame of an Argon Plasma.

that AlO predominates over Al_2O in a neutral or oxidizing atmosphere (see Section 3.2). Thus it is quite credible that the Al_2O_3 dissociates to AlO and O as it is heated in the plasma. The AlO in turn quickly dissociates to Al and O, which explains the absence of detectable AlO in the plasma core. The formation of AlO in the cooler regions also means that any quench process aimed at recovering Al from the plasma must either be rapid enough to prevent significant formation of AlO or provide a reducing agent to preferentially react with the oxygen.

10.4 Identification of Product

The rigorous group III qualitative chemical analysis of product obtained from the reduction of Al_2O_3 in an argon plasma gave positive tests for Al and Fe. The test for aluminum was quite strong whereas that for Fe was weak. The presence of Al in the product was confirmed by an x-ray diffraction analysis. The only diffraction lines in addition to the Al lines were due to α-Al_2O_3, γ-Al_2O_3 and the impurities that were present in the reactant alumina. The Al diffraction line at $2\theta = 38.5°$ and the adjacent α-Al_2O_3 line are presented in Figure 12. Since these lines overlap somewhat, the missing portions of each have been sketched.

It is certain from the above results that Al is the reduction product of Al_2O_3 instead of a solid aluminum suboxide. This Al was found to be highly pyrophoric and finely divided. It is also definite that Fe is present to interfere with the quantitative analysis for Al. Since Fe_2O_3 is much more easily reduced than TiO_2 or ZrO_2 (see

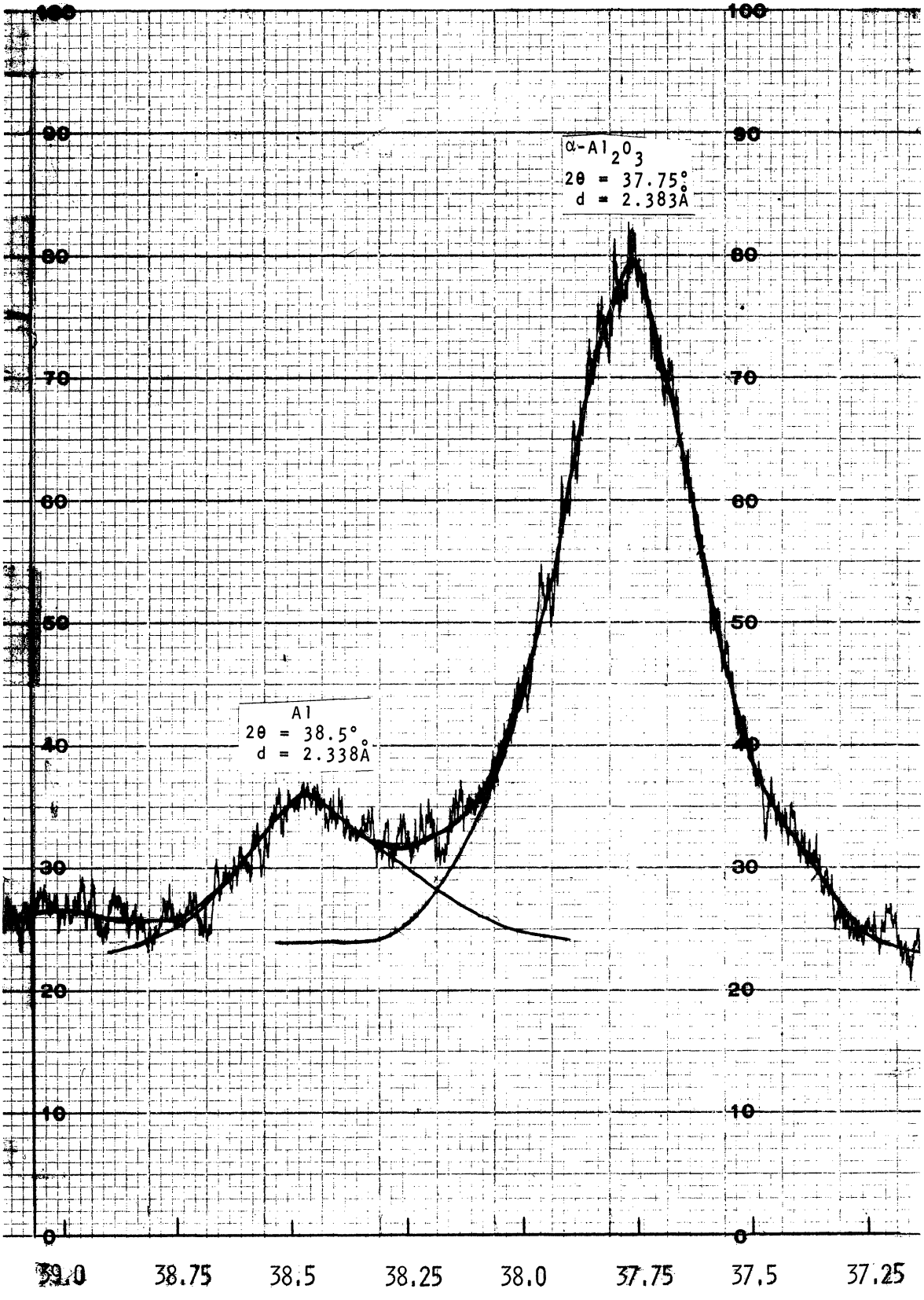

Figure 12. X-Ray Diffraction Lines of Al and α-Al_2O_3 Obtained from the Product of the Reduction of α-Al_2O_3 in an Argon Plasma.

Section 2.1), and since the amount of Fe is much less than the Al, it is probable that Ti and Zr are not present to a significant extent in the product. Zirconium can definitely be neglected because of the very low concentration of ZrO_2 in the original alumina.

Samples obtained from the reduction of Al_2O_3 in Ar-CO and Ar-CH_4 plasmas were also analyzed to determine the nature of the products. Both gave positive qualitative tests for aluminum with the "aluminon-reagent" and both contained a considerable amount of carbon. Diffraction analysis of the product from the Ar-CO reduction identified Al, α-Al_2O_3 and γ-Al_2O_3. Similar analysis of the product from the Ar-CH_4 reduction indicated that Al_4C_3 was present in the sample. The aluminum oxycarbides, Al_2OC and Al_4O_4C, were not found in either case nor were solid aluminum suboxides.

10.5 Accuracy of Aluminum Determinations

Extreme accuracy was not attempted for the quantitative determinations of aluminum in the product. The alumina mass flow rate varied enough during an experimental run, sometimes by as much as ± 15 percent, that it was sufficient to know the Al content within 5 percent. The bromate method for determination of Al was checked with measured volumes of a solution containing a known amount of Al. The solution was prepared by dissolving 1.012 gm of Al powder in HCl and diluting to 1 liter. These checks were performed prior to and during the time that experimental runs were being made.

The aluminum in the known samples was determined within 1.4 to 2.5 percent of the correct amount. The value obtained was always

less than the correct value. Therefore, the aluminum determined in the reduction products should have been within 2.5 percent of the amount actually present, assuming that the contaminants Fe and Ti had no effect. Since these metallic impurities would show up as Al in the bromate method, their presence should give a high value for the amount of aluminum in a sample.

To ascertain the influence of Fe and Ti , a 10 ml sample of the solution obtained by reacting the product from a run with HCl was treated to remove Fe and Ti . The remaining solution was found to contain 2.73 mg Al while 2.62 mg Al were found in 10 ml of solution from which Fe and Ti had not been removed. This variation of ± 2 percent from the average was within the desired accuracy limit and it was decided to forego removal of Fe and Ti in the later work. Subsequent results obtained with duplicate samples also gave variations as high as ± 2 percent from the average (duplicate samples were used for the final experimental runs). In view of the above results, it is felt that the aluminum determinations were easily within the desired 5 percent accuracy limits and in most cases were within 3 percent.

10.6 Effect of Alumina Flow Rate and Particle Size

The alumina mass flow rate and particle size were varied while holding the power input level and argon flow rates constant. The experimental runs were of a two minute duration. The time limit was dictated by the effect of the build-up of solids on the reactor wall, which was determined from the results of runs of different duration, presented in Table IV. They show that the greater the amount of solids collected on

the reactor wall, the lower the percent conversion of the alumina. These results could not be explained by the variation in the alumina flow rate. So in order to determine the effect of varying this flow rate, the subsequent runs were of a constant time length. Since very low flow rates were planned, at least two minute runs were necessary to collect sufficient product for analysis.

TABLE IV

EFFECT OF SOLIDS BUILD-UP

Run Length (min)	Alumina Flow Rate (gm/min)	Total Solids Collected (gm)	Percent Conversion
0.5	0.72	0.25	2.6
1.0	0.39	0.39	2.5
2.0	0.60	0.84	1.9
4.0	0.70	1.95	1.8

Three particle sizes: 500 mesh (26μ), 400 mesh (37μ) and 320 mesh (45μ); and alumina flow rates ranging from 0.03 to 0.60 gm/min were used in the study. The power input to the plasma was 5.03 kw and the axial (solids carrier gas), coaxial and tangential argon flow rates were 2.5, 3.7, and 45.4 gm/min respectively. The variation of percent conversion with alumina flow rate for the three particle sizes is shown in Figure 13. A single run was also made with 60 mesh (250μ) alumina flowing at 0.19 gm/min. There was no aluminum in the product nor was there any spectroscopic evidence of gaseous Al in the plasma. The

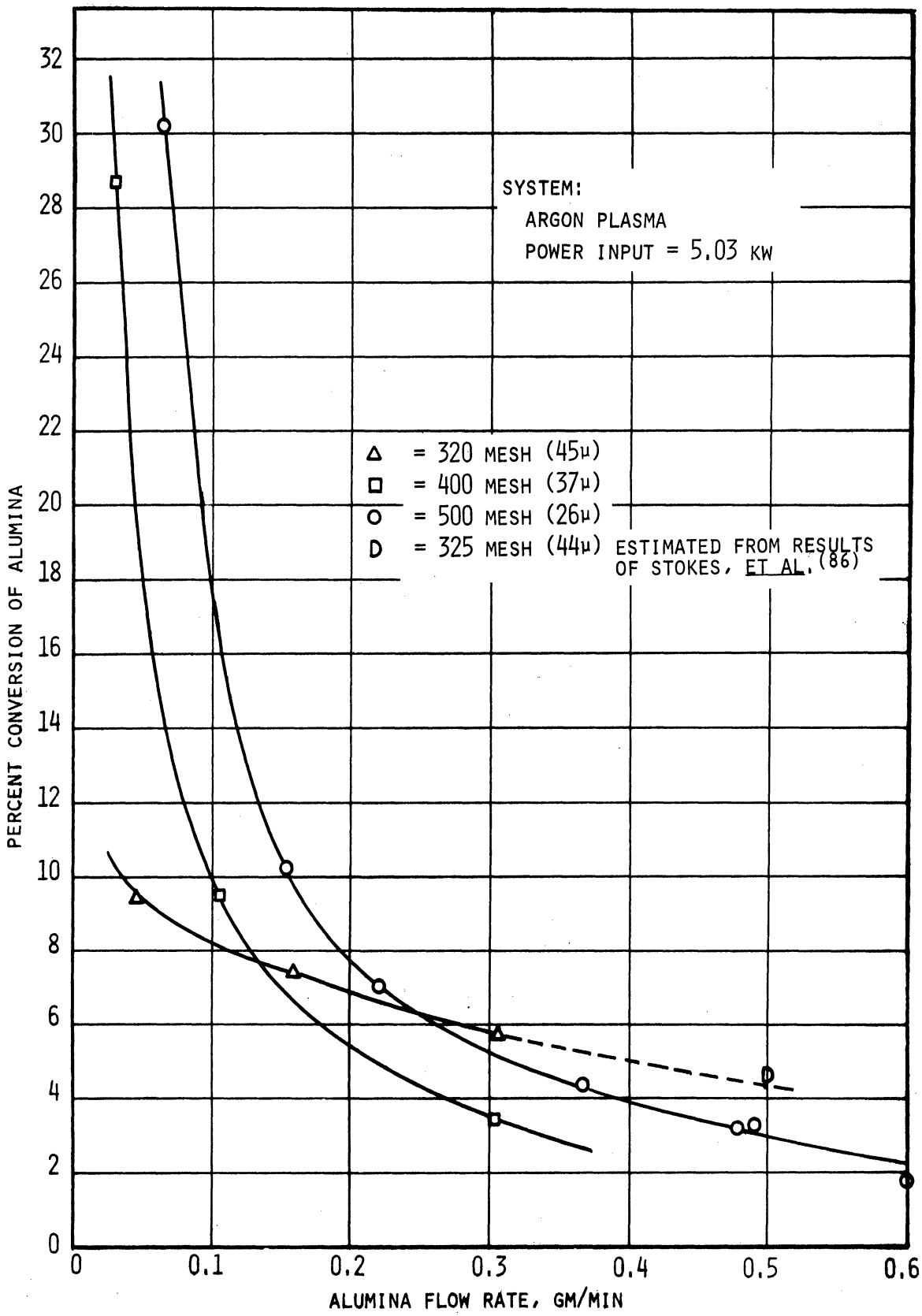

Figure 13. Variation of the Conversion of Al_2O_3 to Al in an Argon Plasma with the Al_2O_3 Flow Rate and Particle Size.

conversion of alumina for this study was based upon the amount of aluminum and alumina collected on the reactor wall.

As expected, the 500 mesh oxide gave a higher conversion than the 400 mesh alumina throughout the entire range of flow rates that were used. This is logical because a smaller 500 mesh particle vaporizes more completely than a 400 mesh particle under the same conditions.

The increase in conversion with a decrease in solids flow rate, exhibited by both 500 and 400 mesh alumina, is also reasonable. The lower the alumina mass flow rate, the fewer particles are present in any section of the plasma at a given time. This means that energy is transferred from the plasma to each particle more efficiently as there is less interference due to nearby particles. As the oxide flow rate increases, the hindrance to the heat transfer becomes greater and the particles are less thoroughly vaporized. When the flow rate of solids is sufficiently great a larger load is presented to the generator and the plasma begins to be affected. Eventually, the plasma is extinguished unless the power input is increased.

The anomalous behavior of the largest particles (320 mesh) can be explained. Taken by themselves, the results for 320 mesh oxide are reasonable as the increase in conversion with decrease in oxide flow rate is exhibited. In addition, the high flow rate result agrees well with the conversions obtained for 325 mesh alumina by Stokes, et al.,[86] as is shown in Figure 13. Since Stokes and his associates did not correlate conversion with alumina flow rate, the point in Figure 13 attributed to them is their highest conversion (5 percent) at their lowest oxide flow rate (0.5 gm/min). Since a helium plasma was used,

which requires considerably more power than argon for comparable plasma temperatures and heat transfer, their 11.6 kw power input is not significant. This was confirmed experimentally. A helium-argon plasma (0.33 gm/min He and 51.6 gm/min Ar) required 5.33 kw for stability while a pure argon plasma flowing at 51.6 gm/min was stabilized with 5.03 kw. But the use of helium and the higher power input did not improve the conversion of alumina. The addition of H_2 to the plasma flame (as the oxide carrier gas) by Stokes and his co-workers is similar to the quench studies of this work because the H_2 did not pass through the arc. It is shown in Section 10.9 that this also does not greatly increase the conversion.

The intersection of the conversion versus flow rate curve for 320 mesh with the curves for 400 and 500 mesh alumina at higher flow rates is explained by the relative extent of hindrance to the heat transfer. As the particle diameter increases, the number of particles at a given mass flow rate decreases. So there are fewer 320 mesh particles in a given volume of plasma at any time and the heat transfer from the plasma is more efficient. As the alumina flow rate decreases, this effect is less noticeable and the curves intersect.

At very low oxide flow rates, single particle flow is approached and an increase in conversion with decrease in diameter is clearly exhibited. The conversions obtained at low flow rates agree qualitatively with the extents of vaporization predicted by the computer solutions to the heat, mass and momentum balances. The comparison of the computer and experimental results is given in Section 10.11.

10.7 Effect of Power Input

The effect of the power input to the plasma was determined by varying the power at a constant alumina flow rate of 0.23 gm/min. Power inputs of 5.03, 5.86 and 6.69 kw and 500 mesh alumina were used. The argon flow rates were the same as in Section 10.6.

The variation of conversion with power input is given in Figure 14. The increase in conversion with an increase in power input was due to two phenomena. First, the argon temperature and the energy content of the plasma were greater. As a result, the particle was more completely vaporized and the concentration of aluminum in the plasma was greater. Second, the aluminum temperature was higher so that the aluminum had a greater diffusivity. (The temperature results are given in Section 10.10) It was shown in Section 5.2 that both effects increase the molar flux of Al to the quench surface. Consequently, the rise in the conversion at the higher power levels was expected. As in Section 10.6, the conversion of alumina was based upon the amount of aluminum and alumina collected on the reactor wall.

10.8 Effect of Reducing Gases in the Plasma

Single runs were made with each of the reducing gases (H_2, CO and CH_4) added to argon plasmas. The same argon flow rates as in Sections 10.6 and 10.7 and 500 mesh alumina were used in the study. The results are presented in Table V along with the results for argon plasmas at comparable alumina flow rates and power levels. Only the aluminum and alumina that collected on the reactor was considered.

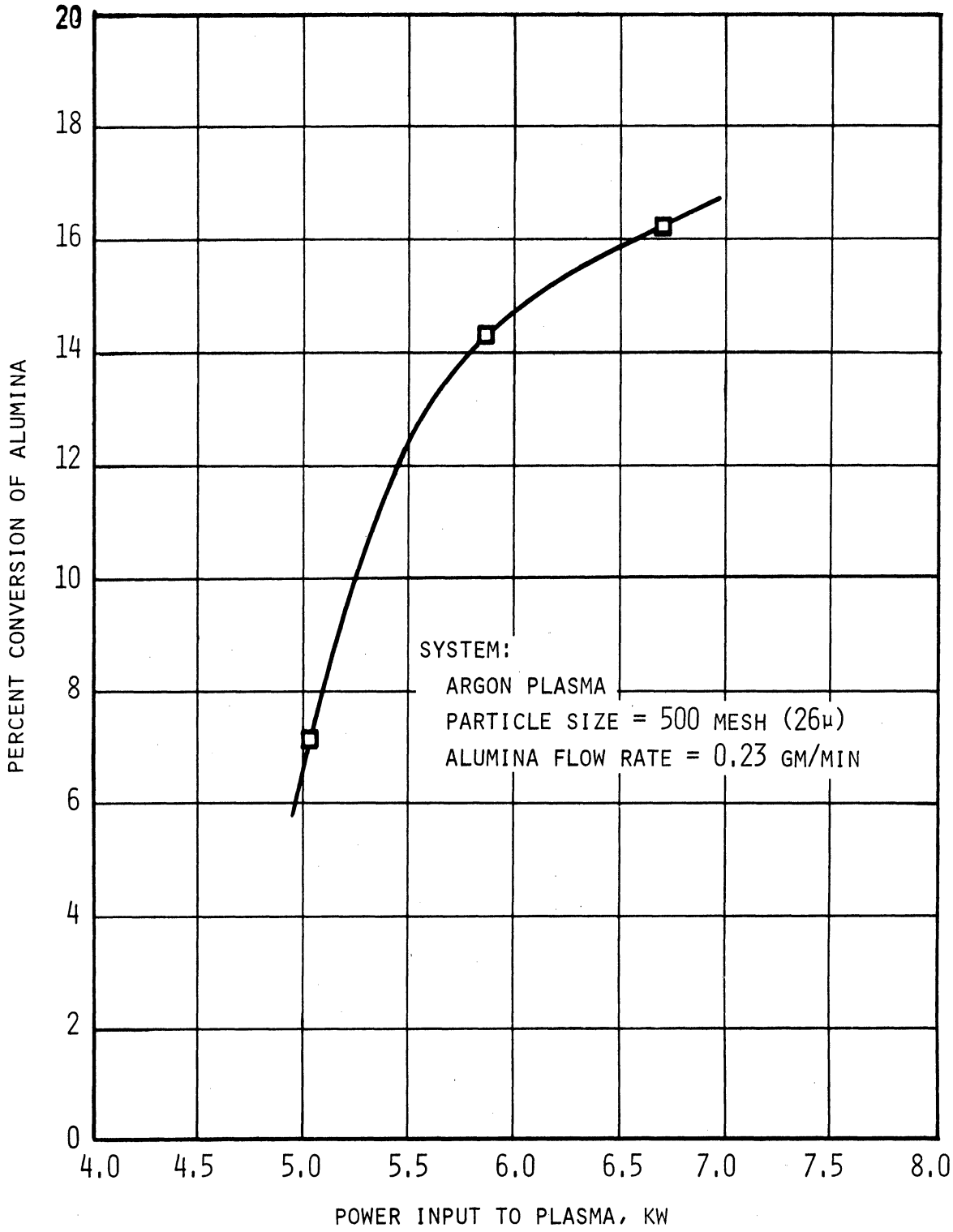

Figure 14. Effect of Power Input Upon the Conversion of Al_2O_3 to Al in an Argon Plasma.

TABLE V

EFFECT OF H_2, CO AND CH_4

Gas	Gas Flow (gmol/min)	Alumina Flow Rate (gm/min)	Power Input (kw)	Percent Conversion of Alumina
H_2	0.045	0.17	5.53	22
CO	0.016	0.15	5.63	46
Ar	---	0.16	5.58	23
CH_4	0.025	0.17	5.03	42
Ar	---	0.17	5.03	9

It was predicted in the discussion in Section 5.1 that hydrogen would not greatly increase the conversion of alumina and that carbon would be of considerable benefit. This is confirmed by the results obtained with H_2, CO and CH_4. Hydrogen had no noticeable effect while carbon monoxide nearly doubled the conversion obtained with argon alone. At a lower power level with methane the conversion was more than quadrupled.

It appears that methane is more effective than carbon monoxide. When CO is dissociated, oxygen is added to the system. So some of the beneficial effect due to the carbon is negated by the additional oxygen. Since carbon condenses easily from the gas phase it is more likely to be in the quench region than oxygen. As a result, the conversion of the alumina is increased despite the extra oxygen. Methane, however, provides carbon without the introduction of oxygen. Furthermore, the study

of CO and CH_4 as quench gases indicated that methane dissociated more easily than carbon monoxide.

10.9 Quench Methods

The alumina conversions reported in Sections 10.6 through 10.8 were based upon the amount of aluminum and alumina collected on the reactor wall, as it was not attempted to recover all the product from the plasma. Water-cooled quench probes and different quench gases were then used in separate experiments to show that the recovery of product could be augmented while maintaining or improving the conversions obtained in the previous studies under the same operating conditions. Argon plasmas, with the same flow rate as in Sections 10.6 through 10.8, a power input of 5.03 kw and 500 mesh alumina were used for the quench studies.

The conversions based upon the material collected on water-cooled quench probes are compared with the conversions obtained with the product collected on the reactor wall in Table VI. It is clear that the quench probes can be used not only to recover additional product but also to increase the conversion. The results obtained with the two larger quench probes can be explained by the discussion in Section 5.2. The probes were placed directly in the plasma, where the aluminum concentration and temperature are the highest. Therefore, the molar flux of Al to the quench probe surface is greater than the flux to the reactor wall. In addition, the distance through which the Al must diffuse to be quenched is less for a probe in the plasma. The result is that greater conversions are obtained with the product collected on the quench probes.

The result for the smallest probe do not contradict the above argument. With the 0.148 in O.D. probe, the alumina flow rate was sufficiently great that the vaporization of the oxide was fairly incomplete. Therefore, the probe was in contact with a much larger number of molten alumina particles than the other probes. These molten particles collect on the probe and build up a layer of solids that inhibits the quenching of aluminum (see Section 10.6). The reactor wall, however, was not in as intimate a contact with the unvaporized alumina as the probe was and so the conversions in the two cases were about the same.

TABLE VI

CONVERSIONS OBTAINED WITH QUENCH PROBES

Quench Probe O.D. (in)	500 Mesh Alumina Flow (gm/min)	Percent Conversion	
		Reactor Wall	Quench Probe
0.148	0.47	3.1	2.9
0.250	0.22	7.1	20
0.375	0.21	7.7	16

The quench gases (H_2, CO, and CH_4) were introduced into the lower section of the plasma core countercurrent to the plasma flow. The purpose was to see what effect these gases would have upon the conversion of the product collected on the reactor wall. The material obtained on the probes, through which the gases were fed, was not analyzed.

The results obtained with four different hydrogen flow rates are presented in Table VII. These conversions are compared with those

for zero hydrogen flow in Figure 15. The amount of hydrogen used was not important and the use of any hydrogen as a quench increased the conversion only slightly.

TABLE VII

EFFECT OF HYDROGEN-QUENCH FLOW RATE

Hydrogen Flow Rate (gmol/min)	500 Mesh Alumina (gm/min)	Percent Conversion of Alumina
0.13	0.58	3.0
0.21	0.17	10
0.39	0.27	6.7
0.58	0.17	10

The conversions achieved with CO and CH_4 as quench gases are compared in Table VIII. In both cases, carbon was deposited on the reactor wall, but considerably more was obtained with methane. However, both CO and CH_4 produced about the same percentage improvement in the conversion.

TABLE VIII

EFFECT OF CO AND CH_4 AS QUENCH GASES

Quench gas	Quench Gas Flow (gmol/min)	500 Mesh Alumina Flow (gm/min)	Percent Conversion of Alumina
CO	0.10	0.15	26
	0.0	0.15	10
CH_4	0.12	0.16	19
	0.0	0.16	9.4

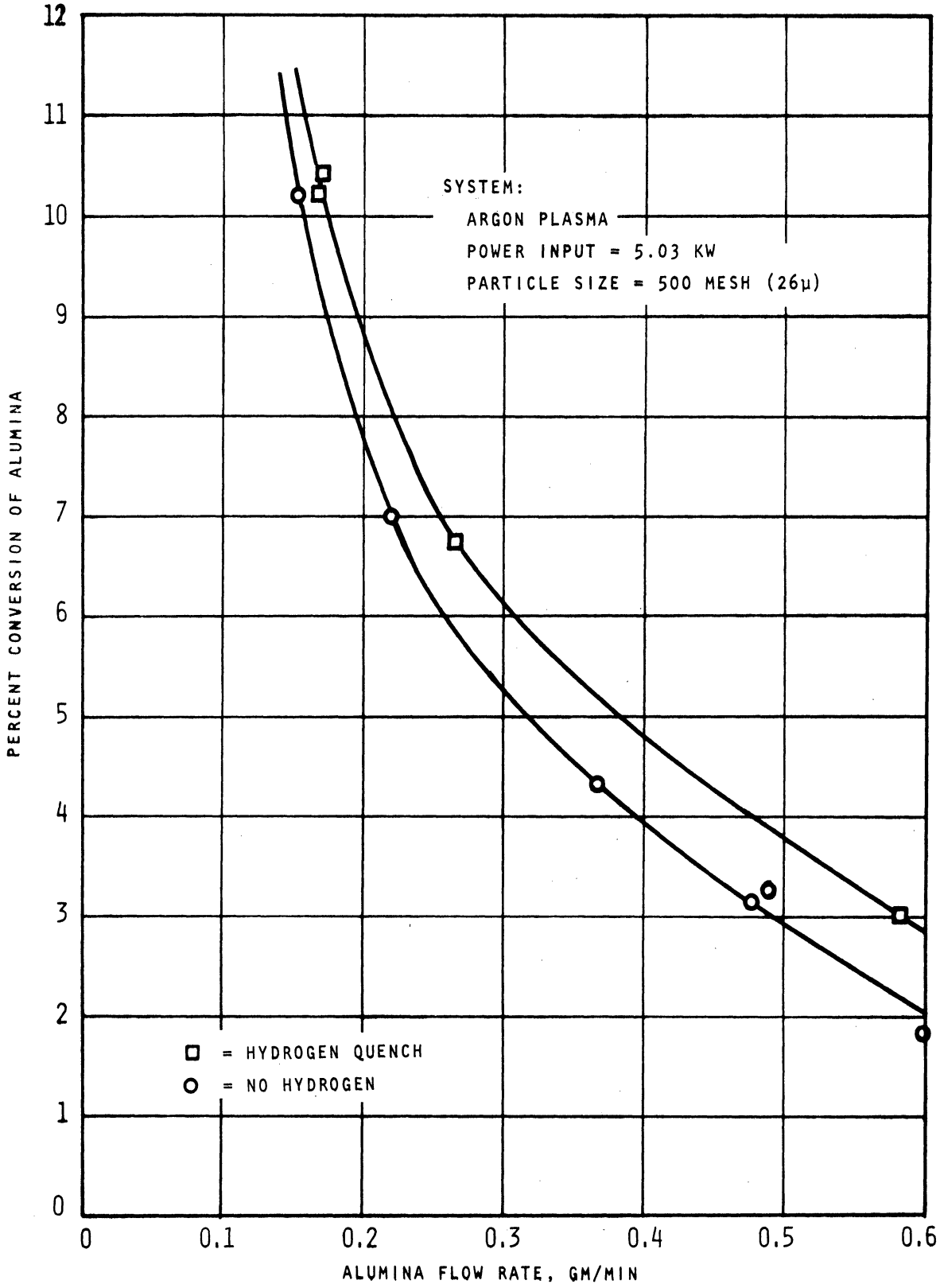

Figure 15. Comparison of Conversions Obtained With and Without the Use of Hydrogen as a Quench Gas.

The effect of any quench gas is to lower the temperature of the aluminum (see Section 10.10). But the diminished aluminum diffusivity is counteracted by the presence of a reducing atmosphere to react with some of the oxygen. This decreases the formation of AlO and Al_2O during the quench and more Al is recovered. It was shown in Section 5.1 that carbon has a much greater affinity for oxygen than hydrogen does. So the more effective quenching by CO and CH_4 in comparison with H_2 is reasonable.

10.10 Argon and Aluminum Temperatures

Argon temperatures were determined at the three power levels of Section 10.7. The temperatures, presented in Table IX, are averages of the values obtained using the 4158.59 and 4259.36 Å Ar_I lines. The enthalpies of atmospheric argon plasmas at these temperatures are also given. It is seen that while the argon temperatures increased only 3 percent, the enthalpy became 10 percent greater.

TABLE IX

ARGON TEMPERATURE AND ENTHALPY

Power Input (kw)	Argon Temperature (°K)	Plasma Enthalpy[28] (cal/gm)
5.03	10,900	1900
5.86	11,100	2030
6.69	11,200	2100

Aluminum temperatures, which were obtained for most of the experimental runs of this work, are given in Table X. The temperatures are generally low and inconsistent. For example, the aluminum temperature should increase as the alumina flow rate decreases. The results for 500 mesh alumina do not exhibit this behavior throughout the range of flow rates studied. The temperatures obtained for the 400 and 320 mesh oxide, however, are consistent. The poor quality of the aluminum temperatures is due to the nature of the silver images obtained on the spectrographic plates. In most cases, the images of the 3944.03 and 3961.53 Å Al_I lines were so dense that complete line profiles were not obtained. So in order to determine the intensity of the lines, the missing portions had to be estimated (see Appendix VI). The inaccuracies inherent in the "multi-line" method (Section 6.4) also add to the deviations. Figure 16 shows a typical plot of $\ell n(I/\nu gA)$ versus E for determination of the aluminum temperatures.

Despite the poor results, it is possible to derive some qualitative information from the aluminum temperatures. The use of a quench gas lowers the temperature of the aluminum as does the use of He or H_2 in the plasma. Higher aluminum temperatures are obtained at greater power input levels and lower alumina flow rates. Any other conclusions would be conjecture.

10.11 Solution of Heat, Mass and Momentum Balances

The computer solutions of heat, mass and momentum balance equations for aluminum oxide particles in an argon plasma are compared with the experimental results at low flow rates. The equations were

TABLE X

ALUMINUM TEMPERATURES

Alumina Flow Rate (gm/min)	Aluminum Temperature (°K)	Remarks*
0.58	2000	H_2 quench, 0.13 gmol/min
0.27	3000	H_2 quench, 0.27 gmol/min
0.17	2800	H_2 quench, 0.58 gmol/min
0.15	3200	CO quench, 0.10 gmol/min
0.15	2600	He in plasma, 5.33 kw
0.17	3200	H_2 in plasma, 5.53 kw
0.49	3000	
0.37	4400	
0.23	4100	
0.23	5200	5.86 kw
0.23	5200	6.69 kw
0.21	3500	
0.16	5900	5.58 kw, complete profiles used
0.06	3900	
0.33	4200	400 mesh
0.31	5100	320 mesh, complete profiles used
0.05	6100	320 mesh, complete profiles used

*Unless otherwise stated, 500 mesh alumina and 5.03 kw were used; and the 3944.03 and 3961.53 Å Al_I line profiles had to be completed.

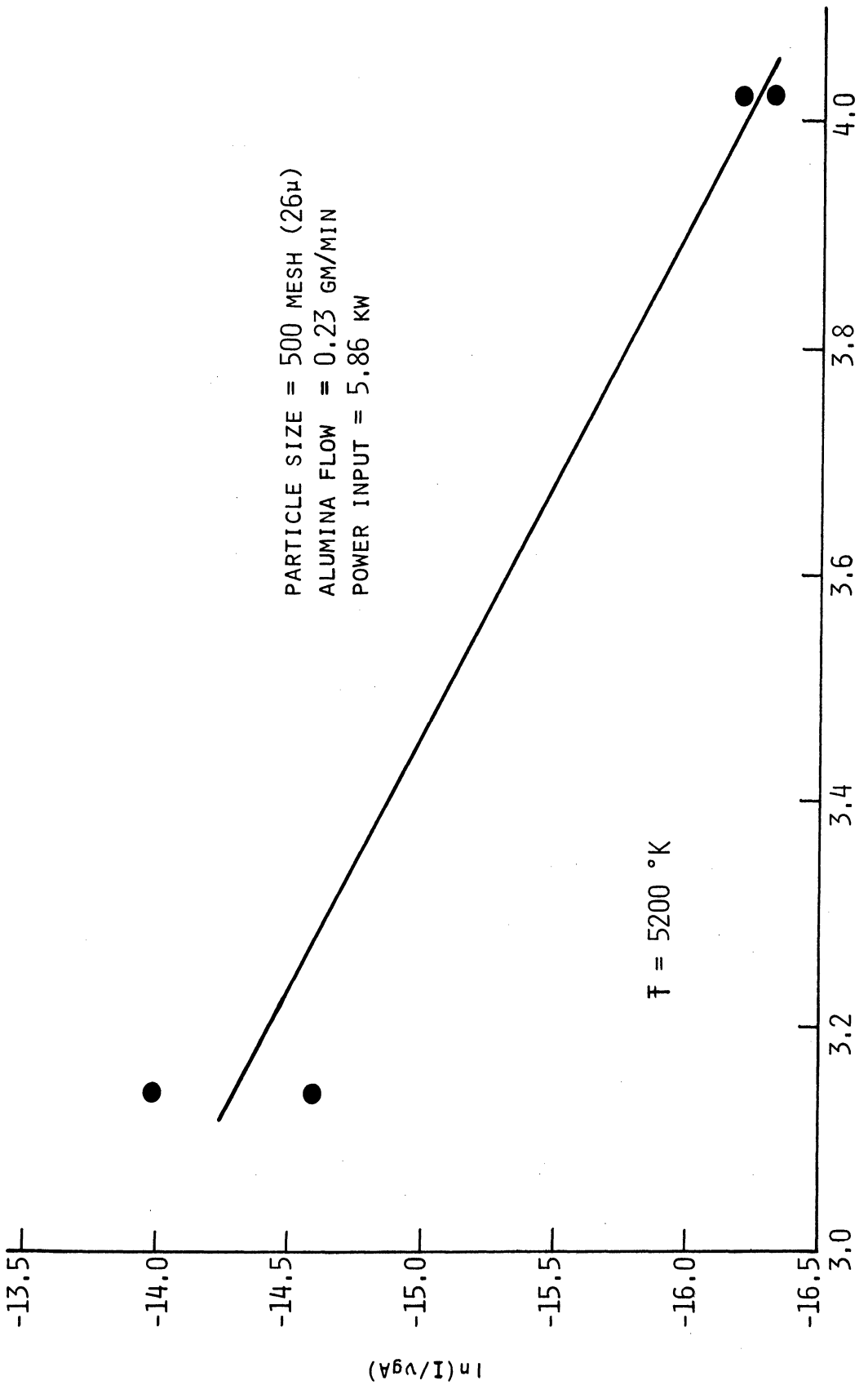

Figure 16. Determination of Aluminum Temperature by the "Multi-Line" Method.

solved for various particle sizes and for 500 mesh alumina at higher power levels. The comparison is made with the results from low solids flow rates because at higher flow rates, the particles begin to interfere with heat transfer to each other. The assumption that the particle surfaces were uniformly accessible for heat and mass transfer was used in the derivation of the equations.

The computer solutions estimate the amount of alumina that will vaporize. This is reported as percent vaporized, which is 100 times the volume vaporized divided by the initial volume for a spherical particle. The conversions predicted for 320, 400 and 500 mesh alumina at a flow rate of 0.06 gm/min (taken from Figure 13) are compared with the percents vaporized, determined for the same plasma conditions, in Figure 17. Since the two curves have the same shape, it appears that a constant fraction of the vaporized aluminum is recovered. It can be concluded that the conversion of alumina increases as more is vaporized. Since this is true for an argon plasma with collection of aluminum on the reactor wall, it has been proven that the recombination of aluminum and oxygen during the quench is less important than the extent of vaporization of the alumina. Apparently, the condensation of aluminum occurs more rapidly than the diffusion of oxygen in the same direction so that once the Al is cooled sufficiently, it leaves the oxygen behind.

The percents of conversion and vaporization are also presented in Table XI for the three particle sizes. The table includes the results obtained with 60 mesh (250μ) alumina and those obtained by Gross, et al.,[47] with 200 mesh (74μ) alumina. This comparison further demonstrates the increase in the percent vaporization achieved with a decrease in particle

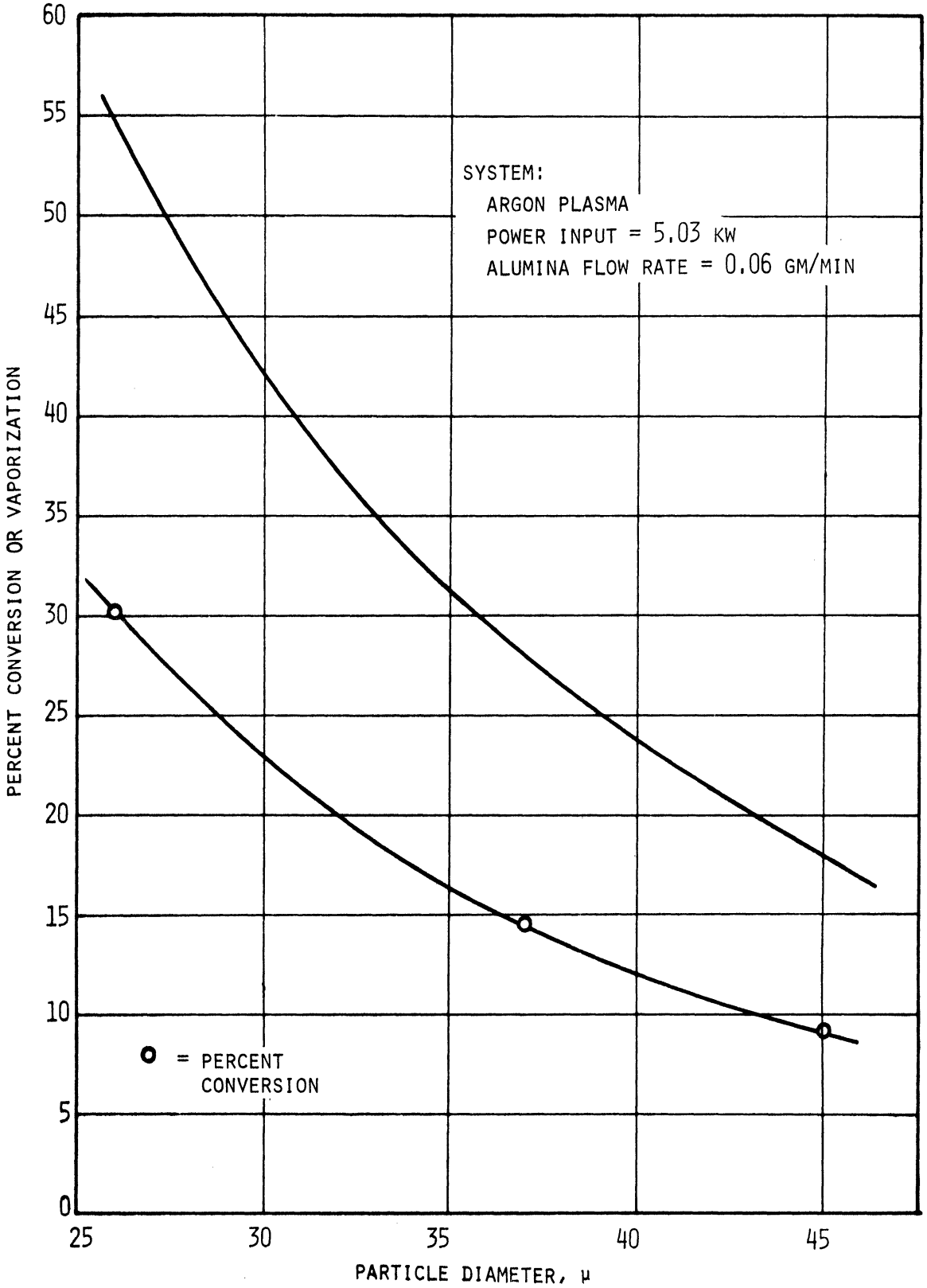

Figure 17. Comparison of the Percents of Conversion and Vaporization Obtained with 26μ, 37μ and 45μ Al_2O_3 Particles.

diameter. It explains the poor results obtained by Grosse and his associates; they simply did not produce enough gaseous Al . The effect of the particle diameter also indicates that much higher conversions than those obtained in this work are possible with smaller particles. For example, the computer solution for 5μ aluminum oxide predicts complete vaporization.

TABLE XI

PERCENTS CONVERSION AND VAPORIZATION FOR VARIOUS PARTICLE SIZES

Particle Size (Mesh)	(μ)	Percent Conversion	Percent Vaporization
500	26	31	54.6
400	37	14	27.7
320	45	9.0	17.6
200	74	0.2-1.25[47]	1.86
60	250	0.0	0.0

TABLE XII

PERCENTS CONVERSION AND VAPORIZATION AT VARIOUS ARGON TEMPERATURES

Argon Temperature (°K)	Percent Conversion	Percent Vaporization
10,900	7.1	54.6
11,100	14	59.7
11,200	16	62.1

The percent vaporization for 500 mesh alumina with the three power levels of Section 10.7 is compared with the experimental conversion in Table XII. (The argon temperature instead of the power input is given.) The increased vaporization due to the higher plasma temperatures and energy contents does not alone explain the size of the conversion increments. Because the aluminum temperatures are also higher in the greater energy plasmas (see Section 10.10), the combination of the two effects can account for the increases in the conversion, as explained in Section 10.7.

Residence times calculated for the different particles are given in Table XIII. These times are less than those reported by Grosse, et al.,[47] as they did not consider vaporization, which decreases the residence time. Since the smaller particles spend less time in the plasma and yet are more completely vaporized, the particle diameter is a more important variable than the residence time.

TABLE XIII

RESIDENCE TIMES FOR ALUMINA PARTICLES

Particle Size (Mesh)	Residence Time (Millisecond)
500	2.19
400	2.57
320	2.88
200	3.94
60	9.14

Previous investigations of heat transfer to solids in plasmas produced heat transfer coefficients of 87-162 and 4000 BTU/hr-ft^2-°F for heat transfer to thermocouple tips (0.02 in O.D.) and small copper slugs respectively (see Sections 2.4 and 3.3). The heat transfer coefficients for this study were calculated with Equation (5.13). The plasma properties used in this correlation were those corresponding to the reference temperature (see Section 5.3), which increased as the solid surface temperature rose. So the heat transfer coefficient continuously increased until the vaporization temperature was reached. At this point the reference temperature remained constant, but the particle diameter began to shrink and the heat transfer coefficient continued to rise. So in order to compare the calculated coefficients with those given above, the values obtained with the particle at its vaporization temperature, but before vaporization has commenced, are assumed to be representative. These coefficients are presented in Table XIV for several particle diameters.

TABLE XIV

CALCULATED HEAT TRANSFER COEFFICIENTS FOR SMALL ALUMINA PARTICLES

Particle Diameter (mesh)	(μ)	Heat Transfer Coefficient (BTU/hr-ft^2-°F)
2500	5	23,300
500	26	4,480
400	37	3,150
320	45	2,590
200	74	1,570
60	250	370

The coefficients calculated for the 320, 400 and 500 mesh particles are on a par with those reported for the small copper slugs. The value obtained for 60 mesh (0.01 inch) agrees well with the 87-162 BTU/hr-ft^2-°F range for the 0.02 inch O.D. thermocouple tips. It is concluded that the heat transfer coefficients used in this study are reasonable. Since the calculated particle residence times are also quite acceptable, the predicted vaporizations should be fairly accurate.

11. SUMMARY AND CONCLUSIONS

The reduction of aluminum oxide to aluminum in an atmospheric, induction-coupled argon plasma flowing at 52 gm/min was studied experimentally. The conversion of the alumina was based upon the amount of Al_2O_3 and Al collected on the reactor wall. The variation of conversion with alumina particle size, alumina mass flow rate and the power input to the plasma was determined. Particle sizes of 500 mesh (26μ), 400 mesh (37μ) and 320 mesh (45μ); flow rates of 0.03 to 0.6 gm/min; and power inputs of 5.03, 5.86 and 6.69 kw were used. These power levels correspond to argon temperatures of 10,900°, 11,100° and 11,200°K respectively. With argon plasmas, the conversions (ranging from 3 to 30 percent) were generally found to increase with decreasing alumina flow rate and particle size and with increasing power input. The improvements in the conversion were due to increases in the percent of the oxide vaporized. The results agree qualitatively with the amount of alumina vaporization predicted by computer solutions to heat, mass and momentum balances for the oxide. The conversions obtained can be explained on the basis of a diffusion controlled quench of aluminum atoms.

The use of water-cooled probes placed directly in the plasma allowed the recovery of additional aluminum at higher conversions. This indicates that with a reactor designed to collect a maximum amount of product, the conversions obtained in this work will be maintained or even improved. It was also possible to enhance the conversion by using CO and CH_4 in the plasma with the argon and as quench gases introduced into the lower section of the plasma core countercurrent to the

plasma flow. Doubling and quadrupling of the conversion was obtained in this way. The use of H_2 in each application was of little benefit. The relative effect of C and H_2 as oxygen scavengers explains the results.

Wet chemical and x-ray diffraction analyses of the reduction product from Ar and Ar-CO plasmas identified Al, α-Al_2O_3 and γ-Al_2O_3. Similar analyses of product from an Ar-CH_4 plasma indicated that Al and Al_4C_3 were present in addition to the oxides. No solid aluminum suboxides or aluminum oxycarbides were found.

It was determined that Al_2O_3 vaporizes in an argon plasma to AlO and O. The AlO in turn quickly dissociates to Al and O. Recombination of Al and O during the quench was not as important a consideration as the percent of the Al_2O_3 vaporized.

Mean aluminum temperatures ranging from 2000 to 6000°K were determined for various operating conditions. The results were generally low and inconsistent. However, it was ascertained that the Al temperature generally increased with increasing power input and decreasing alumina flow rate.

The reduction of aluminum oxide with appreciable conversion has been demonstrated to be quite feasible in an induction-coupled plasma reactor. It should be possible, on the basis of the results of this study, to achieve equal success in the reduction of other metallic oxides that are as stable as alumina.

APPENDIX I

DERIVATION OF MOLAR FLUX OF Al IN QUENCH ZONE

When steep concentration and temperature gradients are involved, the radial diffusion of component i in a mixture is given by:[8,35]

$$N_{ir} = - CD_{im}\left(\frac{\partial X_i}{\partial r} + \frac{k_T}{T}\frac{\partial T}{\partial r}\right) + X_i \sum_{j=1}^{n} N_{jr} \qquad (I.1)$$

where N_{ir} = radial molar flux of i ,

X_i = mole fraction of i ,

D_{im} = effective binary diffusivity for diffusion of i in a mixture,

k_T = thermal diffusion ratio (D_T/D_{im}), where D_T is the thermal diffusivity,

C = total concentration,

T = absolute temperature.

The three terms on the right represent the ordinary diffusion, thermal diffusion and bulk flow contributions respectively.

For low concentrations of species i (as is encountered for Al in this work), k_T is given by:

$$k_T = bX_i \qquad (I\text{-}2)$$

where the constant b does not exceed 0.2 through 0.3.[35] The value of k_T is also far less for gas pairs with close molecular weights. So despite the steep temperature gradients, thermal diffusion can be

neglected. Deleting the thermal diffusion term and rearranging Equation (I.1) gives:

$$N_{ir} = - \frac{C\, D_{im}}{1-X_i} \frac{\partial X_i}{\partial r} + \frac{X_i}{1-X_i} \sum_{\substack{j=1 \\ j \neq i}}^{n} N_{jr} \,. \qquad (I.3)$$

Consider the condensation of component i from a mixture when the other gases are noncondensable. Since these other gases do not condense, the term in Equation (I.3) due to their bulk flow is neglected:

$$N_{ir} = - \frac{C\, D_{im}}{1-X_i} \frac{\partial X_i}{\partial r} \qquad (I.4)$$

This is the equation used in Section 5.2 to describe the condensation of Al from an argon plasma.

APPENDIX II

DERIVATION OF HEAT, MASS AND MOMENTUM BALANCE EQUATIONS FOR AN ALUMINA PARTICLE

The heat, mass and momentum balance equations, which were solved to give an approximate description of an alumina particle as it passed through an argon plasma, are derived in this section. The validity of the assumptions used in these derivations is discussed in Section 5.3.

The velocity and axial position of the particle at a given time are governed by the momentum balance

$$M_s \frac{d^2z}{dt^2} = (\pm F_d + F_g - F_b) g_c \qquad \text{(II.1)}$$

where M_s = mass of a solid particle,

F_g = gravitational force on the particle,

F_b = buoyancy force due to the gas,

F_d = drag force exerted on the particle.

Assuming a spherical particle, Equation (II.1) becomes:

$$\frac{\pi}{6} d_s^3 \rho_s \frac{d^2z}{dt^2} = \pm \frac{1}{2} C_D \frac{\pi}{4} d_s^2 \rho_\infty \left(\frac{dz}{dt} - v_\infty\right)^2 + \frac{\pi}{6} d_s^3 \rho_s g\left(1 - \frac{\rho_\infty}{\rho_s}\right) . \qquad \text{(II.2)}$$

Since $\rho_\infty / \rho_s << 1$, this simplifies to:

$$\frac{d^2z}{dt^2} = \pm \frac{3}{4} C_D \frac{\rho_\infty}{d_s \rho_s} \left(\frac{dz}{dt} - v_\infty\right)^2 + g \qquad \text{(II.3)}$$

where $\frac{dz}{dt}$ = velocity of solid particle,

ρ_s = density of solid particle,

d_s = diameter of solid particle,

ρ_∞ = density of bulk plasma,

v_∞ = velocity of bulk plasma,

g = gravitational acceleration,

C_D = drag coefficient.

Thus the two forces acting on the particle are gravity and drag. Magnetic drag and slip flow effects were negligible.

As a particle is heated in a plasma, energy is transferred to the particle primarily by conduction and convection and is lost from the particle to the surroundings by radiation. In this simplified model, the particles are at a uniform temperature (thermal conduction in the particle was not considered) and vaporization does not commence until the vaporization temperature is reached. The steady state heat balance for particles being heated to the vaporization temperature is:

$$\left[N \rho_s \frac{\pi}{6} d_s^3 C_{p_s}(T_s - T_{ref})\right]_z - \left[N \rho_s \frac{\pi}{6} d_s^3 C_{p_s}(T_s - T_{ref})\right]_{z+\Delta z}$$

$$+ h\left(\frac{S}{V}\right)(T - T_s)\, A\, \Delta z - \sigma e_s \left(\frac{S}{V}\right) T_s^4\, A\, \Delta z = 0 , \qquad \text{(II.4)}$$

where C_{p_s} = heat capacity of solid,

T_s = temperature of solid,

T = temperature of plasma,

z = axial distance along the reactor,

h = conductive and convective heat transfer coefficient,

σ = Stefan-Boltzmann constant,

e_s = emissivity of solid,

N = flow rate of particles (particles per unit time),

A = plasma cross-sectional area,

S/V = particle surface area per unit volume of plasma,

T_{ref} = reference temperature for particle enthalpy.

In the limit, Equation (II.4) becomes:

$$- \frac{d}{dz}\left[N \rho_s \frac{\pi}{6} d_s^3 C_{p_s}(T_s - T_{ref}) \right] + h(\frac{S}{V})(T-T_s)A$$

$$- \sigma e_s (\frac{S}{V}) T_s^4 A = 0 . \qquad \text{(II.5)}$$

The quantity S/V is given by

$$\frac{S}{V} = \frac{N \pi d_s^2}{A \, v_s} \qquad \text{(II.6)}$$

where v_s = velocity of solid, (dz/dt).

Combining Equations (II.5) and (II.6) and using the assumptions of constant particle flow rate and diameter as well as average heat capacity and density for the solid yields:

$$- \frac{1}{6} \rho_s d_s C_{p_s} \frac{dT_s}{dz} + \frac{h(T-T_s)}{v_s} - \frac{\sigma e_s T_s^4}{v_s} = 0 . \qquad \text{(II.7)}$$

And since $v_s = dz/dt$:

$$\frac{1}{6} \rho_s d_s C_{p_s} \frac{dT_s}{dt} = h(T-T_s) - \sigma e_s T_s^4 . \qquad \text{(II.8)}$$

This equation gives the time-temperature history of the particle as it is heated to its vaporization temperature.

When the alumina particle reaches the vaporization temperature (where it essentially dissociates to Al and O), its heat balance is:

$$h \frac{S}{V} (T-T_s)A - \sigma e_s \frac{S}{V} T_s^4 A = \Delta H_r^\circ r_d A , \qquad (II.9)$$

where ΔH_r° = heat of reaction for dissociation to Al and O ,

r_d = rate of dissociation.

It is assumed that the vaporization of the particle proceeds uniformly so that the particle remains spherical. The loss of mass by dissociation is described by:

$$\left[N \rho_s \frac{\pi}{6} d_s^3\right]_z - \left[N \rho_s \frac{\pi}{6} d_s^3\right]_{z+\Delta z} = r_d A \qquad (II.10)$$

In the limit, this becomes:

$$-N \rho_s \frac{\pi}{2} d_s^2 \frac{d(d_s)}{dz} = r_d A \qquad (II.11)$$

It follows from Equations (II.6), (II.9) and (II.11) that:

$$-\frac{1}{2} \Delta H_r^\circ \rho_s \frac{d(d_s)}{dt} = h(T-T_s) - \sigma e_s T_s^4 . \qquad (II.12)$$

This equation, along with Equation (II.3), gives the extent of vaporization of the particle at a given axial position in the plasma.

APPENDIX III

CALIBRATION OF SA1 PLATES

III.1 Background

When a spectrographic plate is exposed to the radiation from a plasma, a silver image is deposited on the plate for each spectral line. The intensity of a given line can be determined from the density of its image. Since the amount of silver deposited is a non-linear function of both line intensity and wavelength, a plate (or emulsion) calibration is necessary before the intensity of a line can be determined. The transmittance or reflectance of light due to the optical components of the scanning system and the spectrograph diffraction grating are also functions of wavelength. This effect can be included in the calibration.

III.2 Calibration Procedure

The combined calibration was done with the use of a tungsten ribbon filament lamp, which was a source with a spectral intensity that was known as a function of wavelength. Ideally, the lamp should be positioned so that its rays would follow the same optical path as radiation from the plasma and so that the spectrograph slit would subtend the same solid angle of radiation from either source. That is, the lamp should be mounted at the reactor site. For the wavelengths used in this study, however, the tungsten continuum intensity was too weak to give silver images dense enough for the calibration to cover spectral lines of normal intensity. Therefore, it was necessary to mount the tungsten lamp directly on the optical bench (past all of

the mirrors and one lens). Then the effect of the rest of the optical path (from the reactor site to the point on the optical bench) was determined with the direct read-out system, which could be used to greatly amplify the signals obtained at the reactor site. This was done by comparing the signals obtained at the two places.

A General Electric Company, 6 volt, 108 watt lamp was used. Power was supplied to the lamp by a 120 volt constant voltage transformer (Variac) hooked up to a 117 to 6 volt step down transformer. The apparent temperature of the tungsten ribbon was measured with a Leeds and Northrup disappearing filament optical pyrometer (Cat. No. 8622) which had been calibrated by the National Bureau of Standards. The true temperature was obtained from the apparent temperature by taking into account the emissivity of the tungsten ribbon,[25] the transmittance of the pyrex lamp envelope,[22] an estimated reflectance and the N.B.S. pyrometer correction tables.[73] The temperature was uniform over the central part of the ribbon and this section was much larger than the area focused upon the spectrograph slit. The corrected temperature and the emissivity of the tungsten ribbon were then used in Planck's radiation law to calculate the intensity of the radiation emitted at a given wavelength.

The actual calibration was done by exposing the plate to the tungsten continuum for several time intervals and to radiation from a plasma containing aluminum. The latter was done so that the wavelength at a point on the tungsten continuum exposure could be determined. It was assumed that all exposures having the same intensity-time product, or relative exposure (RE), would produce equal silver densities. This

is known as intensity-time reciprocity and holds for SA1 plates when exposure times of 5 to 300 sec are used.[29]

Second order radiation dispersed by the diffraction grating did not interfere in the 3000-4000 Å region that was studied since the tungsten ribbon had negligible radiation below 3000 Å. In fact, the tungsten radiation was weak enough at 3082.15 Å and 3092.71 Å that complete calibration curves could not be obtained even with the lamp mounted on the optical bench. So the calibration was repeated at these two wavelengths using the continuous spectrum of a hydrogen lamp from a Beckman DU spectrophotometer. The hydrogen lamp was also mounted on the optical bench. Since the hydrogen continuum intensity was not known, the calibration curves were matched with those obtained from the tungsten lamp, as suggested by Quarderer,[76] to give complete calibration curves.

The calibration curves are plots of relative exposure versus silver density (SD), which is the negative of the common logarithm of the fractional light transmittance through the deposit. The silver densities were measured with a recording microphotometer. The emulsion calibration curves, known as Hurter-Driffield characteristic curves, are given in Figure 18 for the lines used for the aluminum temperature determinations.

III.3 Determination of Absolute Line Intensity

As discussed above, the SA1 plates were calibrated with the tungsten lamp mounted on the optical bench. Then the additional transmittance due to the optical system between that point on the bench and the reactor site was determined using direct read-out. The signal

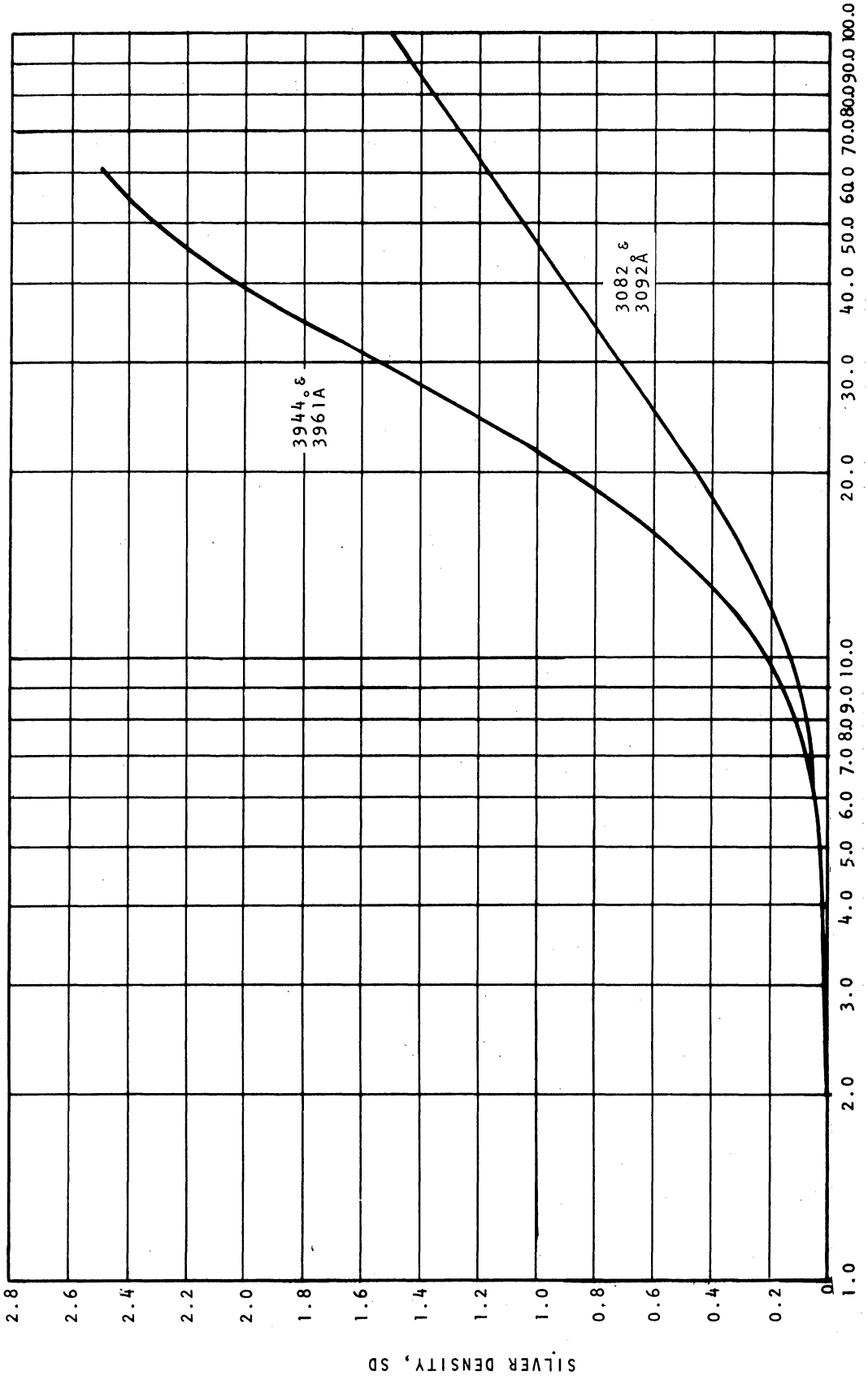

Figure 18. Emulsion Calibration Curves for SA1 Plates.

received by the spectrograph with the lamp on the optical bench is:

$$I_{s_1} = I_w \tau_1 \qquad \text{(III.1)}$$

and the signal from the reactor site is:

$$I_{s2} = I_w \tau_1 \tau_2 \qquad \text{(III.2)}$$

where I_w = intensity of tungsten ribbon,

τ_1 = transmittance of optical system from point on bench to the plate (or phototube),

τ_2 = transmittance of optical system from reactor site to point on beach.

It follows that τ_2 is given by:

$$\tau_2 = I_{s2}/I_{s_1} \qquad \text{(III.3)}$$

The transmittance τ_1 was included in the relative exposures used for the calibration curves (Figure 18), so that

$$RE = RE_w/\tau_1 \qquad \text{(III.4)}$$

where RE = relative exposure used in calibration,

RE_w = relative exposure due to tungsten lamp on optical bench.

When the plate is exposed to plasma radiation, the relative exposure due to a spectral line is:

$$RE_\ell = I_{\ell\lambda}\, \tau_1 \tau_2\, ET\, \tau_s \tau_r \qquad \text{(III.5)}$$

where I_ℓ = relative intensity of spectral line at a given wavelength,

ET = exposure time,

τ_s = transmittance of solids that have collected on the reactor wall,

τ_r = transmittance of clear reactor, i.e. quartz tube, cooling water and pyrex jacket.

If Figure 18 is entered with SD at a point on the spectral line image, then RE_ℓ/τ_1 is obtained. That is:

$$RE_\ell/\tau_1 = RE \ . \tag{III.6}$$

It follows that the relative intensity of the spectral line is given by:

$$I_{\ell\lambda} = RE/\tau_2 \tau_s \tau_r \ ET \ . \tag{III.7}$$

This intensity is a function of the wavelength near the spectral line and the absolute intensity of the line is:

$$I = \int_{-\infty}^{\infty} I_{\ell\lambda} \ d\lambda \ . \tag{III.8}$$

In practice, the integration need not be carried out to infinity as it can be terminated quite near the line center. The integration is discussed in detail in Appendix VI. The transmittances τ_s and τ_r are functions of wavelength and are discussed in Appendix IV.

APPENDIX IV

DETERMINATION OF TRANSMITTANCES OF SOLIDS AND REACTOR

The transmittances τ_s and τ_r, as defined in Appendix III, were determined with the use of the direct read-out system of the spectrograph. With the tungsten lamp mounted on the optical bench, the signals received by the spectrograph with and without the reactor in front of the lamp were compared. This was done with a clear reactor and with various amounts of solids build-up. Since the tungsten radiation passes through the entire reactor and the plasma through only half, this procedure gives τ_s^2 and τ_r^2.

As in Appendix III (for the transmittance of the optical system) we have:

$$\tau_r^2 = I_{s_r}/I_s \qquad \text{(IV.1)}$$

and

$$\tau_s^2 = I_{s_s}/I_{s_r} \qquad \text{(IV.2)}$$

where τ_s = transmittance of solids on reactor wall (in addition to that due to the reactor),

τ_r = transmittance due to clear reactor,

I_{s_r} = signal received through clear reactor,

I_{s_s} = signal received through reactor with solids build-up.

The absolute value of τ_r is easy to determine, but it is impossible to know what τ_s is at a given time during an experimental run because the solids are continuously building up on the reactor wall.

Fortunately, for the aluminum lines used in this work, the ratios $\tau_s(\lambda_2)/\tau_s(\lambda_1)$, $\tau_s(\lambda_3)/\tau_s(\lambda_1)$ and $\tau_s(\lambda_4)/\ _s(\lambda_1)$ were found to be independent of solids build-up. The symbol $\tau_s(\lambda_i)$ refers to the value of τ_s at the wavelength λ_i . This result can be used to advantage since the "multi-line" method, used for determining aluminum temperatures, needs only the relative values of the absolute intensities for the lines. That is, the ratios $I(\lambda_2)/I(\lambda_1)$, $I(\lambda_3)/I(\lambda_1)$, $I(\lambda_4)/I(\lambda_1)$ and 1 can be used just as well as $I(\lambda_1)$, $I(\lambda_2)$, $I(\lambda_3)$ and $I(\lambda_4)$ for the determination. This follows from the fact that T is related to $\ell n(I/\nu gA)$ (See Section 6.4). Therefore, relative values of τ_s and τ_r were used for the aluminum temperature calculations.

APPENDIX V

CALIBRATION OF DIRECT READ-OUT SYSTEM

In order to determine absolute line intensities from the direct read-out of the spectrograph, the photomultiplier tube and optical system had to be calibrated. As for the plate calibration, a 6 volt, 108 watt tungsten filament lamp served as a standard source whose radiant intensity could be calculated. This lamp was mounted at the site of the plasma reactor so that its rays followed the same path as those from the plasma and so that the spectrographic slit subtended the same solid angle of radiation from either source. Then the current output of the photomultiplier tube, at the wavelengths of interest, was compared with the radiant intensity of the tungsten filament. The ratio of the intensity to the current is the spectral response function, $S(\lambda)$, of the multiplier phototube, the electronic circuit and the optical system. The spectral response was a function only of wavelength in this study since the optical system was left unchanged. Calculation of the radiant intensity of the tungsten filament is discussed in Appendix III.2.

APPENDIX VI

CALCULATION OF THE ABSOLUTE INTENSITY OF A SPECTRAL LINE

VI.1 General

The absolute intensity of a spectral line, I, is the integral of the relative intensity, I_λ, over the wavelength interval that contains the line. That is,

$$I = \int_{\lambda_o - \Delta\lambda_B}^{\lambda_o + \Delta\lambda_B} I_\lambda \, d\lambda \,, \qquad \text{(VI.1)}$$

where λ_o = the wavelength at the center of the spectral line,

$\Delta\lambda_B$ = the interval to either side of the line center that contains the particular half of the line profile, i.e. half the width of the base of the profile,

I_λ = relative intensity of the line above the continuum intensity.

The integration should ideally be carried out to infinity but in practicality it is terminated when the relative intensity of the line is indistinguishable from the continuum intensity.

VI.2 Integration of a Spectral Line on a Photographic Plate

When the silver image, which a spectral line caused to be deposited on a spectrographic plate, was scanned with a recording microphotometer a record of silver density versus wavelength was obtained. This was converted to relative intensity above the continuum versus wavelength by referring to the plate calibration curves. Integration of this profile gave the absolute intensity of the spectral line.

Two different situations were encountered in this work. In the first case, a complete profile of relative intensity versus wavelength was obtained. This occurred for all the 3082.15 and 3092.71 Å Al_I lines and the less intense 3944.03 and 3961.53 Å Al_I lines. These curves were divided into several intervals of equal wavelength and the integration over each segment performed by applying Simpson's Rule. The conversion from silver density to relative intensity and the subsequent integrations were done numerically by an IBM 7090 computer.

In the second situation, an incomplete line profile was obtained. This occurred when the spectral line was so intense that the silver density could not be determined near the line center. Such was the case for most of the 3944.03 and 3961.53 Å Al_I profiles obtained, despite the use of exposure times of 3 to 5 seconds. When shorter exposures were made, the 3082.15 and 3092.71 Å Al_I lines were not recorded on the plates.

Since isolated lines of heavier elements have approximate profiles of the Lorentzian shape out into the far wings,[57] it was possible to complete the missing portion of the line profile. The intensities of a known portion of the curve were fitted to a Lorentzian distribution:

$$I(\Delta\lambda) = \left[1 + (\Delta\lambda/\Delta\lambda_{1/2})^2\right]^{-1} \qquad \text{(VI.2)}$$

where $\Delta\lambda$ = the distance from line center,

$\Delta\lambda_{1/2}$ = the (half) half-width of the line,

by the method of least squares. Parameters for the curve fitting were

the intensity of the line at the center of the profile, the continuum intensity and the (half) half-width. The data from the wings of the known curve were not used. A typical result of this analysis is given in Figure 19 for a 3944.03 Al_I line.

VI.3 Integration of Photomultiplier Tube Output

The current output of the photomultiplier tube was passed across a known precision resistor. The resulting voltage was amplified and integrated over the wavelength interval containing the spectral line of interest. The integration was performed directly by an operational amplifier. This integral was then converted to the absolute intensity of the spectral line by multiplying by the spectral response of the direct read-out system at the wavelength of the line.

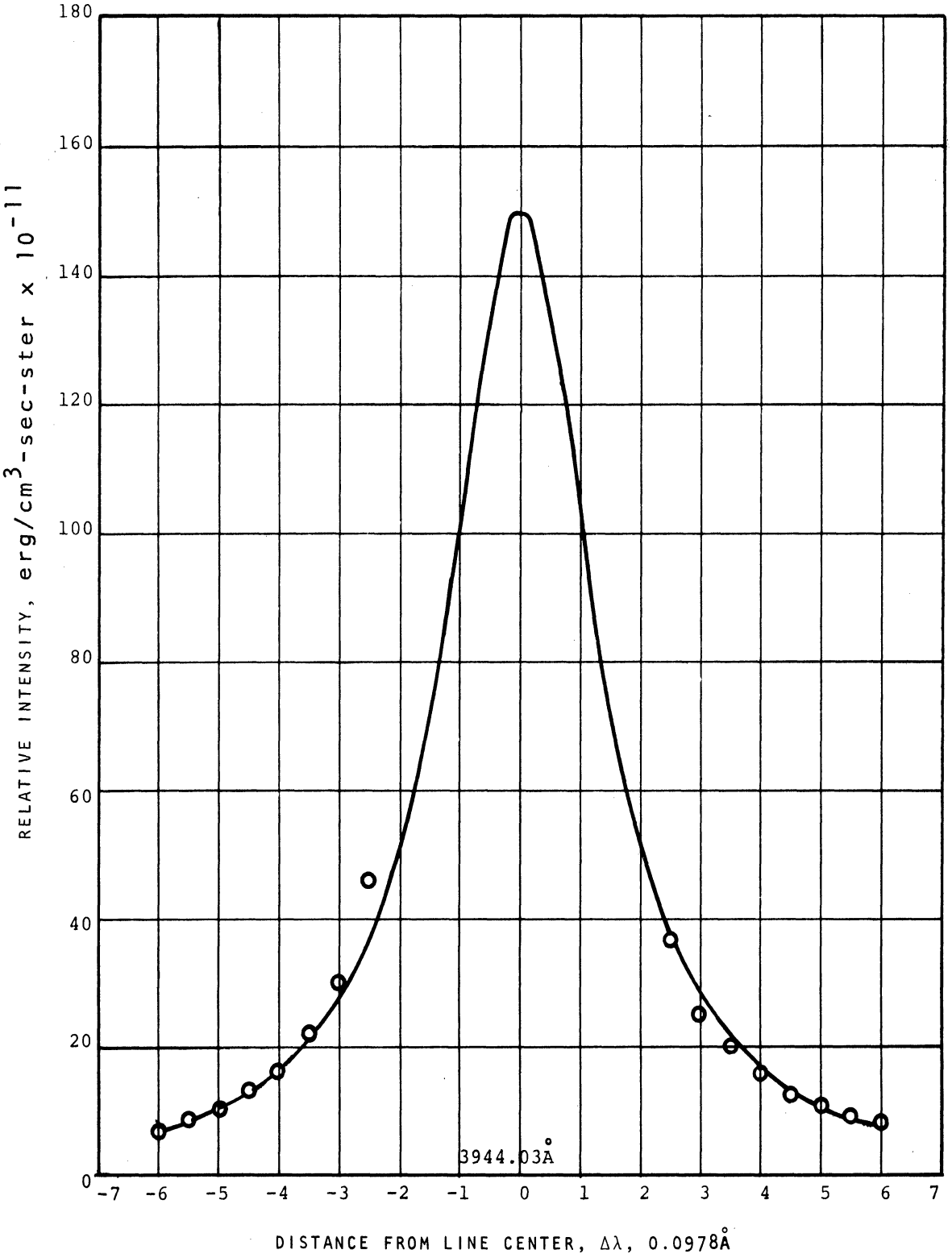

Figure 19. Completion of the Missing Portion of the Intensity Profile of a 3944.03 Å Al_I Line by a Least Squares Fit to a Lorentzian Profile.

APPENDIX VII

SOLUTIONS USED IN VOLUMETRIC DETERMINATION OF ALUMINUM

VII.1 General

The solutions used in the volumetric analysis for aluminum are divided into two groups: those required for the precipitation and dissolution of aluminum quinolate; and those used to determine the resultant 8-quinolinol. The solutions were prepared by dissolving a known weight of substance in a known volume of liquid, unless otherwise stated. All weighings of less than 200 gm (including container) were done on a RIGHT-A-WEIGH balance which is accurate to ± 0.2 mg. Those of over 200 gm were done on a Mettler (Tara 0-2000 gm) balance accurate to ± 0.5 gm.

VII.2 Formation and Dissolution of Aluminum Quinolate

1. 8-Quinolinol (8-hydroxyquinoline; oxine): A 5 wt percent solution of 8-quinolinol in 2M acetic acid. The exact concentration is not important.
2. Tartaric Acid: 10 mg acid/ml solution.
3. Ammonium Acetate: 0.4 gm/ml solution.
4. Bromocresol Purple: 0.04 percent in ethanol.

VII.3 Determination of 8-Quinolinol

1. Bromate-Bromide Solution: 0.1000 N $KBrO_3$ + 100 gm KBr/liter solution. Special care was taken in the preparation of this solution because the $KBrO_3$ was used as a primary standard. The $KBrO_3$ (M.W. = 167.01) used was 100 percent

pure, so 0.1 N $KBrO_3$ is 16.701/6 or 2.7835 gm/l. The bromate was weighed in a crucible, dried at 180°C and 1-1/2 hours, cooled and reweighed.(63) The amount of $KBrO_3$ used for a liter of the solution was 2.7840 gm. The exact KBr concentration is unimportant.

2. Potassium Iodide: 20 wt percent KI in water.

3. Thiosulfate: 0.1 N $Na_2S_2O_3$ solution. Special care was also taken in the preparation of this solution. The thiosulfate was dissolved in freshly boiled (to remove CO_2) distilled water and 0.1 gm Na_2CO_3/liter was added as preservative.(63) Reagent grade (99.5 percent) $Na_2S_2O_3 \cdot 5H_2O$ was used and the normality determined with the primary standard, $KBrO_3$. The thiosulfate normality was checked periodically.

4. Starch Solution: 0.2 percent solution. After suspending 4 gm powdered starch in 600 ml distilled water, 20 percent KOH was added until a thick, almost clear solution was obtained. This was allowed to stand one hour for a complete reaction and then was neutralized to the litmus end point. Glacial acetic acid (2 ml) was added as a preservative and the solution was diluted to 2 liters.

NOMENCLATURE

Symbol	
A	area - cm^2
A_{nm}	Einstein transition probability for spontaneous transition from level n to level m - sec^{-1}
C	total concentration - $gmol/cm^3$
C_D	drag coefficient
C_p	heat capacity - cal/gm-°K
d	diameter - cm,
d	spacing between crystal planes
D_{im}	effective binary diffusivity for diffusion of i in a mixture - cm^2/sec
D_T	Thermal diffusivity - cm^2/sec
e	emissivity
E	Energy - erg
ET	exposure time - sec
F_b	buoyant force - dyne
F_d	drag force - dyne
F_g	gravitational force - dyne
g	gravitation acceleration - cm/sec^2
g	statistical weight
h	heat transfer coefficient - $cal/sec\text{-}cm^2\text{-}°C$
h	Planck's constant - erg-sec
h	specific enthalpy - cal/gm
h_{ref}	specific enthalpy at reference temperature in film around a solid particle - cal/gm

NOMENCLATURE (Continued)

Symbol	
ΔH°_r	heat of reaction - cal/gm
I	absolute intensity of radiation - erg/cm^2-sec-ster
I_s	signal received by spectrograph
k	Boltzmann constant - erg/°K
k	thermal conductivity - cal/sec-cm-°C
k_T	thermal diffusion ratio
L	path length or source thickness - cm
M	mass - gm
N	flow rate of particles - particles/sec
N	number density - cm^{-3}
N_{ir}	radial molar flux of i - gmol/cm^2-sec
P_r	Prandtl number
Q	electronic partition function
r	radial position - cm
r_d	rate of dissociation - gm/cm^3-sec
Re	Reynolds number
RE	relative exposure - erg/cm^3-ster
S	surface area - cm^2
$S(\lambda)$	spectral response of photomultiplier and optical system - erg/cm^2-sec-amp-ster
t	time particle has been in plasma - sec
T	absolute temperature - °K
v	velocity - cm/sec
v_{rel}	velocity of solid particle relative to the plasma - cm/sec

NOMENCLATURE (Continued)

Symbol	
V	volume - cm^3
X_i	mole fraction of i
z	axial position in plasma - cm
ε_ℓ	volume emission coefficient of spectral line - erg/cm^3-sec-ster
2Θ	angle between diffracted x-ray beam and transmitted beam - degrees
λ	wavelength - cm, Å
λ_o	wavelength at center of spectral line - cm, Å
$\Delta\lambda$	distance from line center - cm, Å
$\Delta\lambda_B$	(half) base-width of spectral line - cm, Å
$\Delta\lambda_{1/2}$	(half) half-width of spectral line - cm, Å
ν	frequency of emitted photon - sec^{-1}
ρ	density - gm/cm^3
σ	Stefan-Boltzmann constant - $cal/sec\text{-}cm^2\text{-}°K^4$
τ	transmittance

Subscripts

f	film or boundary layer around a solid particle in plasma
ℓ	spectral line
m	upper energy state
n	lower energy state
r	clear reactor
s	solid particle
w	tungsten filament
0	ground level

NOMENCLATURE (Continued)

Symbol	
1	site of calibration on optical bench
2	site of plasma reactor
∞	bulk plasma

BIBLIOGRAPHY

1. Ackermann, R. J. and R. J. Thorn. "Gaseous Oxides of Aluminum, Tungsten and Tantalum," J. Am. Chem. Soc., 78, 4169 (1956).

2. Allen, William A., John S. Rinehart and W. C. White. "Phenomena Associated with the Flight of Ultra-Speed Pellets. Part I. Ballistics," J. Appl. Phys., 23, 132-37 (1952).

3. Ayres, Gilbert H. Quantitative Chemical Analysis, Harper and Brothers, New York, 1958.

4. Beletskii, M. S. and M. B. Rapoport. Doklady Akad. Nauk S. S. R., 80, 751-4 (1951).

5. Bennett, Carl and Norman L. Franklin. Statistical Analysis in Chemistry and the Chemical Industry, John Wiley and Sons, Inc., New York, 1961.

6. Biggerstaff, G. E., W. R. Golliher, R. L. Harris and W. R. Rossmassler. "Plasma Torch Production of Elemental Boron," AEC R and D Report, KY-453, February 26, 1964.

7. Bildstein, H. "Melting Materials into Spheres with a Plasma Torch," Chem.-Ingr.-Tech., 38, No. 10, 19-25 (1966), see C. A. 64:12211 g.

8. Bird, R. Byron, Warren E. Stewart and Edwin N. Lightfoot. Transport Phenomena, John Wiley and Sons, Inc., New York, 1960.

9. Bowen, Stuart W. "A Spectroscopic Study of an Underexpanded Argon Plasma Jet," Ph.D. Thesis, The University of Michigan, 1966.

10. Brewer, Leo. "The Thermodynamic Properties of the Oxides and their Vaporization Processes," Chemical Reviews, 52, 1-75 (1953).

11. Brewer, Leo and Alen W. Searcy. "The Gaseous Species of the Al-Al_2O_3 System," J. Am. Chem. Soc., 73, 5308-14 (1951).

12. Brown, R. A. S. "Reaction of Some Zirconium Compounds in a Plasma Jet," Presented at the CIMM, Conference of Metallurgists, Kingston, Ontario, August 28-30, (1967).

13. Buchanan, Robert S. "Study of a Seeded Plasma," Ph.D. Thesis, The University of Michigan, Ann Arbor, 1961.

14. Carnahan, Brice, H. A. Luther, James O. Wilkes. Preliminary Edition of Applied Numerical Methods, Vol. I, John Wiley and Sons, Inc., New York, 1964.

15. Chludzinski, George R. "Energy Transfer to Solids in R. F. Generated Plasmas," Ph.D. Thesis, The University of Michigan, Ann Arbor, 1964.

16. Christiansen, E. B. "Effect of Particle Shape on Free Settling Rates," Ph.D. Thesis, The University of Michigan, Ann Arbor, 1943.

17. Cochran, C. Norman. "Aluminum Suboxide Formed in Reaction of Aluminum with Alumina," J. Am. Chem. Soc., 77, 2190-1 (1955).

18. Coheur, F. P. and P. Coheur. Chem. Zentr., 1, 978 (1944).

19. Coheur, F. P. and P. Coheur. Rev. universelle mines, 19, 86-9 (1943).

20. Coheur, P. "Temperature Measurement by Means of Molecular Spectra," Bull. classe sci., Acad. Roy. Belg., 28, No. 7/9, 569-73 (1942).

21. Corliss, Charles H. and William R. Bozman. "Experimental Transition Probabilities for Spectral Lines of Seventy Elements," U.S. National Bureau of Standards, Monograph No. 53, 1962.

22. Corning Glass Works, "Glass Color Filter," Bulletin CF-1, Corning, New York, 1960.

23. Cullity, B. D. Elements of X-ray Diffraction, Addison-Wesley Publishing Company, Inc., Reading, Massachusetts, 1956.

24. De Maria, G., J. Drowart and M. G. Inghram. "Mass Spectrometric Study of Al_2O_3," J. Chem. Phys., 30, 318-19 (1959).

25. De Vos, J. C. "A New Determination of the Emissivity of Tungsten Ribbon," Physica, 20, 714 (1954).

26. Dickerman, P. J. and R. W. Deuel. "Measurement of Relative Transition Probabilities for Some Lines of Cu_I, Al_I, and Mo_I Spectra," Journal of Quantitative Spectroscopy and Radiative Transfer, 4, No. 6, 807-17 (1964).

27. Dow Chemical Company. JANAF Thermochemical Tables, ARPA Proj. AF 04(611)-7554, Midland, Michigan (1965).

28. Drellishak, K. S., C. F. Knopp and Ali Bulent Cambel. "Partition Functions and Thermodynamic Properties of Argon Plasma," Technical Documentary Report No. AEDC-TDR-63-146, August 1963.

29. Eastman Kodak Company. "Kodak Plates and Films for Science and Industry," Kodak Publication No. P-9, Eastman Kodak Company, Rochester, N. Y., 1962.

30. Eckert, E. R. G. "Engineering Relations for Friction and Heat Transfer to Surfaces in High Velocity Flow," Journal of the Aeronautical Sciences, 22, 585-587 (1955).

31. Elliott, John F. and Molly Gleiser. Thermochemistry for Steelmaking, Vol. 1, Addison-Wesley Publishing Company, Inc., Reading, Massachusetts, 1960.

32. Emlin, B. I., B. B. Papin and S. T. Rostovtsev. "The Mechanism of Electrocorundum Reduction by Solid Carbon," Met. i Koksokhim., Mezhvedomistv. Resp. Nauchn.-Tekhn. Sb., 3, 36-40 (1965).

33. Engelke, John L. "Heat Transfer to Particles in the Plasma Flame," Stanford Research Institute, Menlo Park, California, January 30, 1962.

34. Foster, L. M., G. Long and M. S. Hunter. "Reactions Between Aluminum Oxide and Carbon. The Al_2O_3-Al_4C_3 Phase Diagram," J. Am. Ceram. Soc., 39, 1-11 (1956).

35. Frank-Kamenetskii, D. A. trans. N. Thon, Diffusion and Heat Exchange in Chemical Kinetics, Princeton University Press, Princeton, New Jersey, 1955.

36. Gastinger, E. "Preparation of Lower Oxides," Naturwissenschaften, 42, 95 (1955).

37. Gericke, W. E. "Messung der Ubergangswahrscheinlichkeit von AI-linien," Z. Astrophys., 53, 68-79 (1961).

38. Gibbins, S. G. and B. Siegel. "Reduction of Aluminum Oxide by Propellant Combustion Gases at High Temperatures," Report No. TDR-269-(4210-10)-7, Contract No. AF 04(695)-269, September 1, 1964.

39. Ginsberg, H. and V. Sparwald. "Extraction of Aluminum by Carbothermic Reduction with Special Reference to the Aluminum-Carbon System," Aluminium, 41, No. 3, 181-93, No. 4, 219-30 (1965).

40. Gitleson, Gunnar, Oddvin Herstad and Ketil Motzfeldt. "Carbothermic Reduction of Al_2O_3," Selected Topics High Temperature Chemistry, 179-96 (1966), see C. A. 65:9819h.

41. Glassner, Alvin. "The Thermochemical Properties of the Oxides, Fluorides, and Chlorides to 2500°K," Argonne National Laboratory Report No. ANL-5750, Contract W-31-109-eng-38 (1957).

42. Glasstone, Samuel, Keith J. Laidler and Henry Eyring. Ph.D., The Theory of Rate Processes, McGraw-Hill Book Company, Inc., New York 1941.

43. Goldsmith, Alexander, Thomas E. Waterman and Harry J. Hirschhorn. Handbook of Thermophysical Properties of Solid Materials, Vol. 3, The Macmillan Company, New York, 1961.

44. Goodlett, Vernon Wilson. "The Visible and Near Ultraviolet Spectra of the Aluminum Monoxide Molecule," Ph.D. Thesis, Vanderbilt University, August, 1959.

45. Goulden, Cyril H. Methods of Statistical Analysis, Second ed. John Wiley and Sons, Inc., New York, 1952.

46. Griem, Hans R. Plasma Spectroscopy, McGraw-Hill Book Company, New York, 1964.

47. Grosse, A. V., H. W. Leutner and C. S. Stokes. "Plasma Jet Chemistry," First Annual Report, Office of Naval Research, Contract 3085(02), Task No. NR 052-429, December 31, 1961.

48. Grossman, L. N. "Niobium-Al_2O_3 Reactions Yielding Condensed and Volatile Products," J. Chem. Phys., 44, No. 11, 4127-31 (1966).

49. Grube, G., A. Schneider, V. Esch and M. Flad. "Zur Kenntnis des Aluminiumsuboxyds," Z. anorg. Chem., 260, 120-6 (1949).

50. Harrison, George R. Massachusetts Institute of Technology: Wavelength Tables, John Wiley and Sons, Inc., New York, 1939.

51. Hasapis, A. A., M. B. Panish and C. Rosen. "The Vaporization and Physical Properties of Certain Refractories," WADD Technical Report 60-463, Part I, PB 171 413, October 1960.

52. Hedger, H. J., and A. R. Hall. "Preliminary Observations on the Use of the Induction-coupled plasma Torch for the Preparation of Spherical Powder," Powder Metallurgy, No. 8, 65-72, 1961.

53. Herzberg, Gerhard. Atomic Spectra and Atomic Structure, Dover Publications, New York, 1944.

54. Herzberg, Gerhard. Spectra of Diatomic Molecules, D. Van Nostrand Company, Inc., Princeton, New Jersey, 1950.

55. Hoch, Michael and Herrick L. Johnston. "Formation, Stability and Crystal Structure of the Solid Aluminum Suboxides: Al_2O and AlO," J. Am. Chem. Soc., 76, 2560-1 (1954).

56. Hodgman, Charles D., Robert C. Weast, and Samuel M. Selby (editors). Handbook of Chemistry and Physics, 42nd edition, The Chemical Rubber Publishing Co., Cleveland, Ohio, 1960.

57. Huddlestone, Richard H. and Stanley L. Leonard (editors). Plasma Diagnostic Techniques, Academic Press, New York, 1965.

58. Huska, Paul A. and Curtis W. Clump. "Decomposition of Molybdenum Disulfide in an Induction-coupled Argon Plasma," I and EC Process Design and Development, 6, No. 2, 238-244 (1967).

59. Inghram, M. G., W. A. Chupka and J. Berkowitz. "Dissociation Energies from Thermodynamic Equilibria Studied with a Mass Spectrometer," Memoires Soc. Roy. Sci. Liége, Ser. 4, 18, 513-35 (1957).

60. Kempthorne, Oscar. Design and Analysis of Experiments, John Wiley and Sons, Inc., New York, 1952.

61. Khodak, L. P. and V. S. Mal'tsev. Tr. Khim. Met. Inst., Akad. Nauk S. S. R., 1, 218-31 (1963).

62. Kodama, K. Methods of Quantitative Inorganic Analysis, Interscience Publishers, London, 1963.

63. Kolthoff, I. M. and R. Belcher. Volumetric Analysis, Vol. III, Interscience Publishers, Inc., New York, 1957.

64. Levenspiel, Octave. Chemical Reaction Engineering, John Wiley and Sons, Inc., New York, 1962.

65. Loo, S. L. and R. C. Dimick. "Interaction of Solid Particles with an Ionized Gas," Tech. Report ILL-12-p, Project Squid, Cont. Nonr - 3623(00) and NR-098-038, November, 1963.

66. Mal'tev, V. S., V. D. Ponomarev, V. T. Panyushkin and S. M. Isabaev. "The Mechanism of the Thermal Decomposition and Reduction of Sodium and Potassium Hydroaluminates," Tr. Inst. Met. i Obogashch., Akad. Nauk Kaz. S. S. R., 12, 136-142 (1965).

67. Margrave, J. L. "Chemistry at High Temperatures," Science, 135, No. 3501, 345 (1962).

68. Marynowski, C. W. and A. G. Monroe. "R-F Generation of Thermal Plasmas," High Temperature Technology, Butterworths, London, 1964.

69. McAlpine, Roy K. and Byron A. Soule. Fundamentals of Qualitative Chemical Analysis, 4th Edition, D. Van Nostrand Company, Inc., Princeton, New Jersey, 1956.

70. Meyer, H. "Fusion of Powders in a Plasma Jet," Ber. Dtsch. Keram. Ges., 41, No. 2, 112-119 (1964).

71. Motzfeldt, Ketil, Tek. Ukeblad., 109, 1137-42 (1962).

72. Pearse, R. W. B. and A. G. Gaydon. The Identification of Molecular Spectra, John Wiley and Sons, Inc., New York, 1963.

73. Poland, D. E., J. W. Green and J. L. Margrave. "Corrected Optical Pyrometer Readings," NBS Monograph 30, U. S. Government Printing Office, April 21, 1961.

74. Ponomarev, V. D., V. T. Panyushkin and V. S. Mal'tsev. "Mechanism of Physicochemical Transformations in the Thermal Reduction with Carbon of Synthetic Nepheline," Vestn. Akad. Nauk Kaz. S. S. R., 21, No. 7, 32-5 (1965).

75. Porter, R. F., P. Schissel and M. G. Inghram. "Mass Spectrometric Study of Gaseous Species in the Al-Al_2O_3 System," J. Chem. Phys., 23, 339-42 (1955).

76. Quarderer, George J. "Photochemical Chlorination of Sulfur Dioxide Utilizing a Plasma Light Source," Ph.D. Thesis, The University of Michigan, Ann Arbor, April 1967.

77. Reed, Thomas B. "Heat-transfer Intensity from Induction Plasma Flames and Oxyhydrogen Flames," J. Appl. Phys., 34, No. 8, 2266-9 (1963).

78. Rosen, B. Constantes Selectionnées Atlas, Hermann and C^{ie}, Depositaires, Paris, 1952.

79. Rosen, B. Constantes Selectionnées Données Spectoscopiques Concernant Les Molécules Diatomiques, Hermann and C^{ie}, Depositaires, Paris, 1951.

80. Seymour, Errol V. "Particle Injection Techniques for Velocity Measurement in Arc Plasmas," Technical Report No. 12, National Science Foundation Grant GP-414, Harvard University, December, 1964.

81. Sherman, Martin P. and Jerry Grey. "A Technical Report on Calculation of Transport Properties Mixtures of Helium and Partly-ionized Argon," Aeronautical Engineering Laboratory Report No. 673, Princeton University, N. J., December, 1963.

82. Smith, Dean L. "Mass and Energy Transfer Between a Confined Plasma Jet and a Gaseous Coolant," Ph.D. Thesis, The University of Michigan, February, 1965.

83. Smith, Delbert M. "Plasma Spraying of Refractory Materials," General Motors Engineering Journal, 23-28, Second Quarter 1963.

84. Smith Joseph V. (editor) "Index to the X-ray Powder Data File," ASTM Special Technical Publication 48-L, ASTM, Philadelphia, Pa. 1962.

85. Stokes, Charles S. "Chemical Reactions with the Plasma Jet," Chemical Engineering, 191-196, April 12, 1965.

86. Stokes, C. S., J. A. Cahill, J. J. Correa and A. V. Grosse. "Plasma Jet Chemistry," Final Report, Air Force Office of Scientific Research, Contract AFOSR-62-196, December, 1964.

87. Stokes, C. S., W. W. Knipe and L. A. Streng. "Heat Transfer Rates of an Argon Plasma," J. Electrochem. Soc., 107, 35-8 (1960).

88. Walas, Stanley M. Reaction Kinetics for Chemical Engineers, McGraw-Hill Book Company, Inc., New York, 1959.

89. Wood, Bernard J. and Henry Wise. "The Interaction of Atoms with Solid Surfaces," PB Report 156, 822, U. S. Dept. Comm., Office Tech. Serv. (1960).

90. Worrell, W. L. "Carbothermic Reduction of Alumina. A Thermodynamic Analysis," Can. Met. Quarterly, 4, No. 1, 87-95 (1965).

91. Zhadanova, L. V. and V. A. Sokolov. "Structure and Nature of Emission of the Spectrum of Aluminum Oxidation," Zh. Prikl. Spektroskopii, 1, No. 3, 272-5 (1964).